Fossil evidence for a hyperdiverse sclerophyll flora under a non–Mediterranean-type climate

J. M. Kale Sniderman[a,1], Gregory J. Jordan[b], and Richard M. Cowling[c]

[a]School of Earth Sciences, University of Melbourne, VIC 3010, Australia; [b]School of Plant Science, University of Tasmania, Hobart, TAS 7001, Australia; and [c]Botany Department, Nelson Mandela Metropolitan University, Port Elizabeth 6031, South Africa

Edited by Taylor Feild, James Cook University, Townsville, Queensland, Australia, and accepted by the Editorial Board January 4, 2013 (received for review October 1, 2012)

The spectacular diversity of sclerophyll plants in the Cape Floristic Region in South Africa and Australia's Southwest Floristic Region has been attributed to either explosive radiation on infertile soils under fire-prone, summer-dry climates or sustained accretion of species under inferred stable climate regimes. However, the very poor fossil record of these regions has made these ideas difficult to test. Here, we reconstruct ecological-scale plant species richness from an exceptionally well-preserved fossil flora. We show that a hyperdiverse sclerophyll flora existed under high-rainfall, summer-wet climates in the Early Pleistocene in southeastern Australia. The sclerophyll flora of this region must, therefore, have suffered subsequent extinctions to result in its current relatively low diversity. This regional loss of sclerophyll diversity occurred at the same time as a loss of rainforest diversity and cannot be explained by ecological substitution of species of one ecological type by another type. We show that sclerophyll hyperdiversity has developed in distinctly non-Mediterranean climates, and this diversity is, therefore, more likely a response to long-term climate stability. Climate stability may have both reduced the intensity of extinctions associated with the Pleistocene climate cycles and promoted the accumulation of species richness by encouraging genetic divergence between populations and discouraging plant dispersal.

macrofossil flora | species diversity | species-area curve | glacial-interglacial cycles

Mediterranean climate regions support ~20% of vascular plant species on 5% of Earth's surface (1) and show positive anomalies in the latitudinal plant species diversity gradient. Researchers have used two approaches to explain this gradient. The first approach emphasizes the importance of contemporary environmental processes. For example, some models use energy and water availability to explain global patterns of diversity (2, 3). Alternatively, historical models focus on geological-scale processes and often invoke the contrasting antiquity of tropical vs. temperate climates. For example, the tropical conservatism hypothesis (4) argues that the high diversity of tropical floras accumulated over tens of millions of years during warm, ever-wet, early-middle Cenozoic climates. This model infers that temperate floras are depauperate because they were derived relatively recently from a small number of thermophilic lineages that were able to colonize novel temperate climates during the late Cenozoic. However, these contemporary and historical models must neglect or misrepresent important processes, because they fail to predict the richness of the Mediterranean climate biome (2, 5, 6). Hyperdiverse Mediterranean climate regions, therefore, provide a test of current theories about the evolution of global patterns of species richness.

The Mediterranean climate regions are renowned for having sclerophyll floras—floras dominated by tough-leaved, slow-growing, short-statured, often woody taxa at the slow end of the leaf economics spectrum (7). Sclerophylly is particularly important in the most species-rich (on a per-area basis) of these regions, the Cape Floristic Region (CFR) in South Africa and the Southwest Floristic Region (SWFR) in Australia (1) (Fig. 1). The high species richness of SWFR cannot be explained by high topographic heterogeneity, because this region has a very flat, low-elevation landscape (1). Furthermore, CFR, although more mountainous than SWFR, is more elevationally uniform than the remaining three Mediterranean climate regions (1). Instead, authors have invoked soil infertility (5, 8), unusual climate stability at a range of temporal scales (9–11), contemporary landscape and edaphic diversity (8), Cenozoic landscape dynamics (6), or fire (10). However, many of the contemporary features used to explain the hyperdiverse southwestern regions fail to explain patterns of diversity within these continents. The phylogenetically related sclerophyll floras in the southeast Cape and southeast Australia are also exposed to widespread soil infertility, seasonal moisture stress, fire, and high landscape and edaphic diversity, but they are significantly less species-rich (5, 11, 12). Explanations for the sclerophyll hyperdiversity of CFR and SWFR must account for these parallel east–west diversity gradients.

Much of the controversy surrounding the origins of sclerophyll diversity relates to when these biomes became hyperdiverse. Several authors (1, 13, 14) have hypothesized that explosive speciation after the development of Mediterranean climates during the late Cenozoic explains most of the sclerophyll richness in CFR and SWFR. Phylogenetic and fossil evidence indicates much greater ages and progressive subsequent diversification of some of the major sclerophyll clades (5, 9, 15–19), but the timing of the development of species richness in these clades remains unclear. In particular, lower extinction rates than in other extratropical regions could contribute significantly to the greater diversity of CFR and SWFR. However, this idea contradicts the established paradigm that fire-dependent, drought-tolerant sclerophyll floras replaced moisture-dependent, fire-sensitive rainforest during the late Cenozoic (20–22).

If hyperdiverse sclerophyll floras developed in response to environmental features or processes associated with Mediterranean-type climates, we would expect that sclerophyll floras existed only as low-diversity biomes until their diversification was accelerated by the appearance of Mediterranean-type climates. Alternatively, if hyperdiverse sclerophyll floras are primarily a product of geologically long periods of relative environmental stability (9), then currently hyperdiverse regions may be those regions that have experienced the least climate variability over timescales meaningful for speciation. One potential way to resolve this question is to address the fossil record. Almost all of the relevant fossil evidence is based on pollen (5, 10), which shows decreased diversity of rainforest floras and increased abundance of sclerophyll taxa

Author contributions: J.M.K.S. and G.J.J. designed research; J.M.K.S., G.J.J., and R.M.C. performed research; J.M.K.S. and G.J.J. analyzed data; and J.M.K.S., G.J.J., and R.M.C. wrote the paper.

The authors declare no conflict of interest.

This article is a PNAS Direct Submission. T.F. is a guest editor invited by the Editorial Board.

[1]To whom correspondence should be addressed. E-mail: kale.sniderman@unimelb.edu.au.

This article contains supporting information online at www.pnas.org/lookup/suppl/doi:10.1073/pnas.1216747110/-/DCSupplemental.

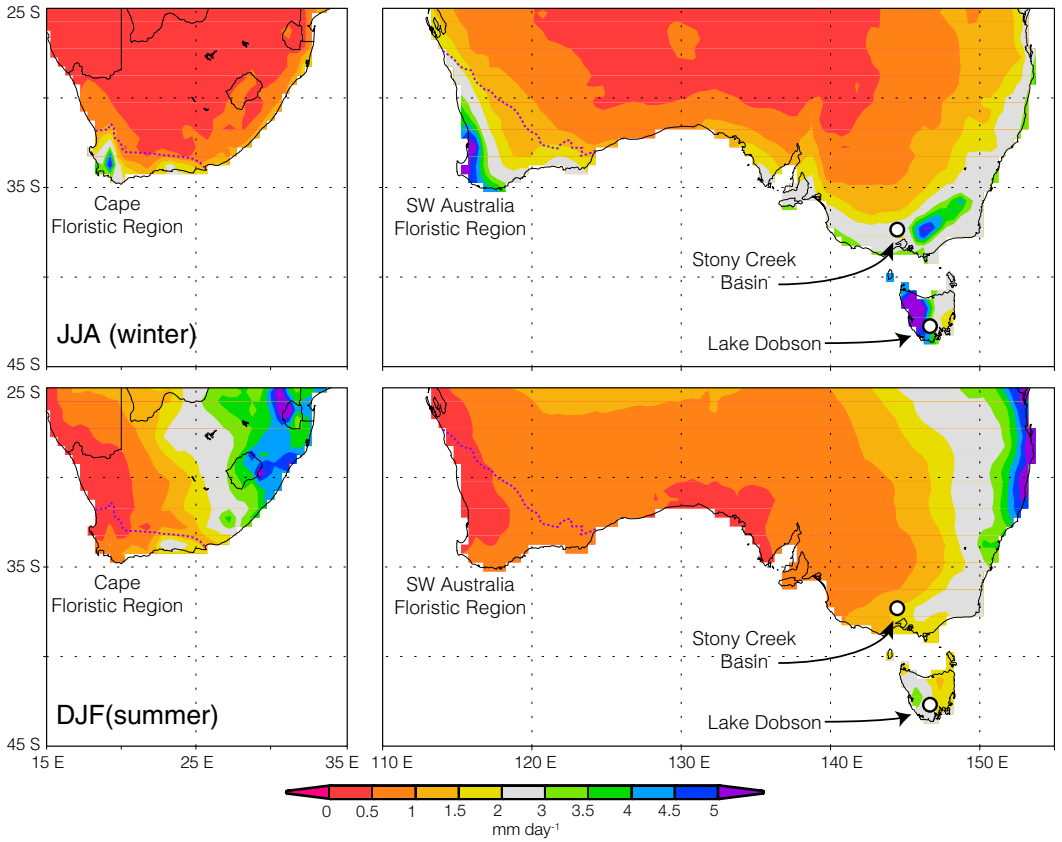

Fig. 1. Southern Africa and southern Australia winter and summer precipitation (millimetres per day), from Climatic Research Unit TS3.10.1 data set.: *Upper*, June to August [1950–2000]; *Lower*, December to February [1950–1999]). Location of the Cape Floristic Region in South Africa and the Southwest Floristic Region in Australia and location of the fossil locality SCB and LD. Precipitation plotted with Climate Explorer (http://climexp.knmi.nl).

during the late Neogene (20, 23). Unfortunately, the fossil pollen record has low taxonomic resolution (typically to the level of genus) and therefore, is poor at detecting species extinctions and radiations, particularly for sclerophyll floras, which exhibit high species richness within genera. As a result, the fossil pollen record provides little basis for characterizing the history of species richness in this biome. However, macrofossils (leaves, flowers, fruits, etc.) have the potential to better address questions of diversity because of their higher taxonomic resolution (24).

Here, we use exceptionally preserved macrofossils recovered from a small paleolake, Stony Creek Basin (SCB), in southeast Australia (Fig. 1) to estimate standing ecological-scale species richness of Early Pleistocene sclerophyll vegetation. We used a model based on the diversity of fossil leaves at SCB and the diversity of leaves deposited in a modern analog system (Lake Dobson, Tasmania). We then compared this inferred species richness with species area curves constructed for SWFR, CFR, and eastern Australia. Our analyses show that a sclerophyll flora with species richness comparable with CFR and SWFR existed during the Early Pleistocene in a relatively mesic region that now has low-diversity sclerophyll floras. Furthermore, the fossils predate the development of current winter-dominated rainfall regimes in southeast Australia: paleoclimatic reconstructions from SCB show annual rainfall ≥ 1.5 times and summer rainfall ~ 2–2.4 times higher than today (25). The SCB fossil flora, therefore, contradicts hypotheses attempting to explain the origins of the hyperdiverse CFR and SWFR floras solely in terms of contemporary Mediterranean climates.

Results

In addition to conifers, ferns, bryophytes, and monocots, we found leaf and stem fossils of 69 sclerophyllous species of dicots in our sample (n = 1,118) of the SCB sediments (Fig. 2 and *SI Appendix*, Figs. S1–S35). Of these species, 43 species were woody sclerophyll taxa typical of Australian sclerophyll floras (*Eucalyptus*, other Myrtaceae, *Acacia*, *Allocasuarina*, *Banksia*, *Hakea*, *Boronia*, Bossieae, and *Bauera*) (Fig. 2), including 19 previously described species of Ericaceae (26). The identification of several of these groups was verified by the presence of reproductive structures [*Acacia* (*SI Appendix*, Fig. S2), *Boronia* (*SI Appendix*, Fig. S3), Ericaceae (*SI Appendix*, Figs. S8–S26), *Eucalyptus*, *Leptospermum*, and *Baeckea* (*SI Appendix*, Figs. S27–S30)]. The remainder could not be placed into groups, because the Australian sclerophyll flora shows high levels of morphological convergence and apart from Proteaceae and Ericaceae (26–29), has poorly known anatomy. For example, superficially similar small, linear entire leaves with tightly revolute margins occur within Proteaceae, Fabaceae, Asteraceae, Lamiaceae, Euphorbiaceae, Ericaceae, Dilleniaceae, Tremandraceae, Frankeniaceae, Rhamnaceae, and Polygalaceae. However, the unidentified leaves were small and thick (*SI Appendix*, Figs. S1–S35), consistent with attributes of woody species. The dominance of the flora by woody species is consistent with strong taphonomic biases against preservation of herbs (30, 31).

The relationship between the species richness in a plant fossil assemblage and the species richness of the source flora is complex and involves three major potential biases. First, fossil assemblages are typically derived from sediment samples laid down over a time period (in our example, ~2,500 y). During this period, the species composition of the source vegetation may have changed (32). Second, collections of species-rich plant macrofossil assemblages typically undersample the diversity present in the sediments from which they are recovered (33–35). Third, the poor preservation potential of most macroscopic plant organs means that fossil leaf

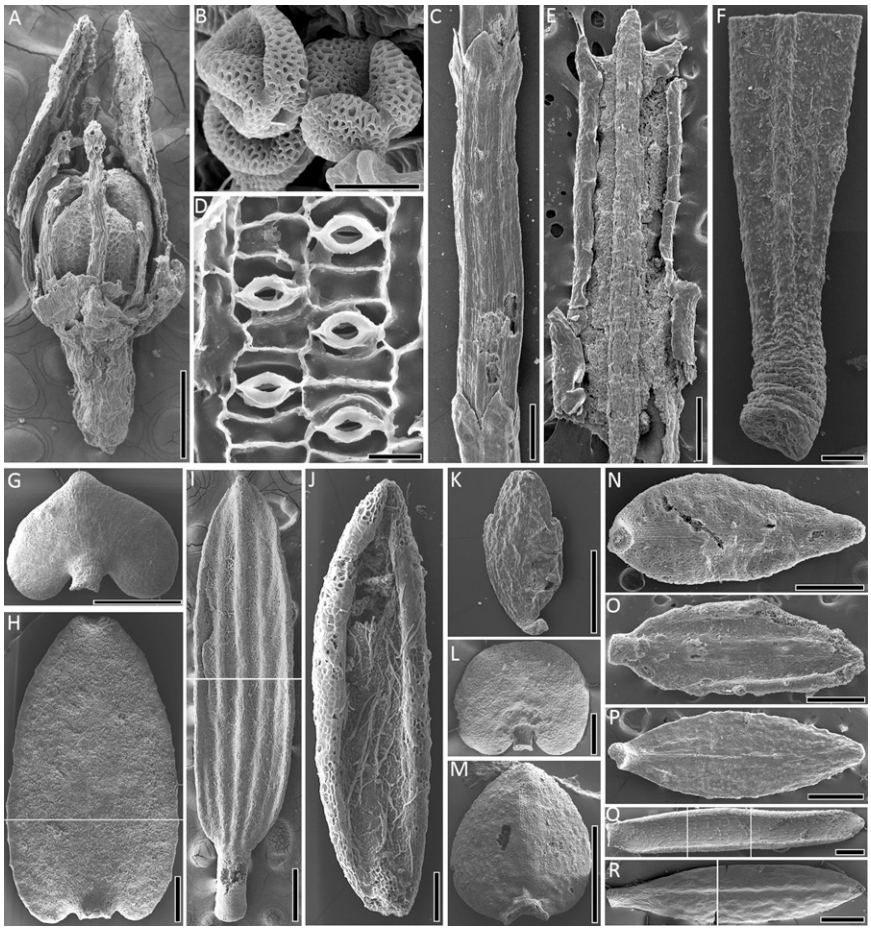

Fig. 2. Scanning electron micrographs illustrating the diversity and excellent preservation typical of fossils from SCB. (*A*) Flower of *Boronia cf parviflora*. (*B*) In situ pollen grains from *A*. (*C*) Foliage fragment of *Allocasuarina cf torulosa*. (*D*) Inner surface of the cuticle of *C* showing stomata and epidermal cells. (*E*) Leaf fragment of *Banksia ericifolia*. (*F*) Phyllode of an *Acacia* species. (*G–I*) Leaves of Ericaceae subfamily Styphelioideae; 20 anatomically distinct morphospecies of this group were present. (*J*) Leaf of Fabaceae *cf* Bossieae. (*K*) *Bauera* sp. (Cunoniaceae). (*L–R*) Unidentified species. *H*, *I*, *Q*, and *R* are composite images as indicated by white lines. (Scale bars: *A*, *C*, *E–R*, 0.5 mm; *B*, 10 μm; *D*, 20 μm.)

assemblages include only a subset of the species present in their source communities, leading to underestimates of the richness of source floras, regardless of investigator effort (31).

We established that the first bias (time averaging) was small as follows. The numbers equivalent β-diversity of the flora, $D(H_\beta)$ (36), estimated from the Shannon diversities of the individual and pooled sediment samples (37) for the SCB fossil samples was 1.03 (*SI Text*), implying that the samples effectively represent only 1.03 distinct communities (36). Resampling of the pooled flora indicated that this estimate was not significantly greater than one ($P = 0.312$). We conclude that species turnover between the four fossil samples is negligible and leads to no significant bias.

To compensate for undersampling of the sediments, we estimated the asymptotic or true richness of the fossil flora using the abundance-based coverage estimator (ACE) (38), which estimates true assemblage richness based on the relative abundances of rare taxa, those taxa with frequencies of one (singletons) up to a user-determined cutoff frequency k (10 in this case). The ACE richness estimate of the fossil flora is 90.5 species [95% confidence interval (CI) = 78.2–119.4] (Table S1), suggesting that the fossil flora, with observed species richness $S = 69$ (including 23 singletons), is strongly undersampled.

To allow for taphonomic undersampling of the source vegetation, we modeled the species richness of the Early Pleistocene SCB source vegetation by reanalyzing the only comprehensive taphonomic study of a species-rich sclerophyll flora (30). We compared assemblages of leaves recovered from surficial sediments of Lake Dobson (LD) with the species composition of LD's potential catchment area (Tables S1 and S2). LD provides a plausible analog for the SCB fossil flora, because the floras are broadly similar in sclerophylly, leaf size, and floristic composition. Also, we can assume similar source areas for leaves for both lakes. Leaves are rarely transported far, except by rivers (31), and high fall velocities strongly restrict the aerial dispersal of sclerophyllous leaves (31). We, therefore, consider that the hydrological catchment areas of ~50 ha at both SCB and LD (*SI Text*) represent the catchments for leaves at these sites.

We then estimated that the 50 ha source vegetation at SCB contained 288 woody dicot species (95% CI = 179–380) by assuming identical ratios between the ACE estimates and species richness of the source vegetation for LD and SCB. Estimates based on rarefaction techniques and estimates using other published southern hemisphere leaf taphonomic studies yielded similar results (240–340 species) (Tables S1 and S2).

Our estimate of SCB 50 ha source vegetation woody species richness (288 species) is significantly greater than the corresponding estimates for southeast Australia (78 species; $F = 72.41$, $P < 0.0001$), SWFR (133 species; $F = 10.18$, $P = 0.002$), and CFR (148 species; $F = 5.68$, $P = 0.022$) (Fig. 3). Our estimate's 95% lower confidence limit (179 species) is significantly higher than the corresponding predicted richness for a similar area in southeast Australia (at $P < 0.001$) but indistinguishable from richness

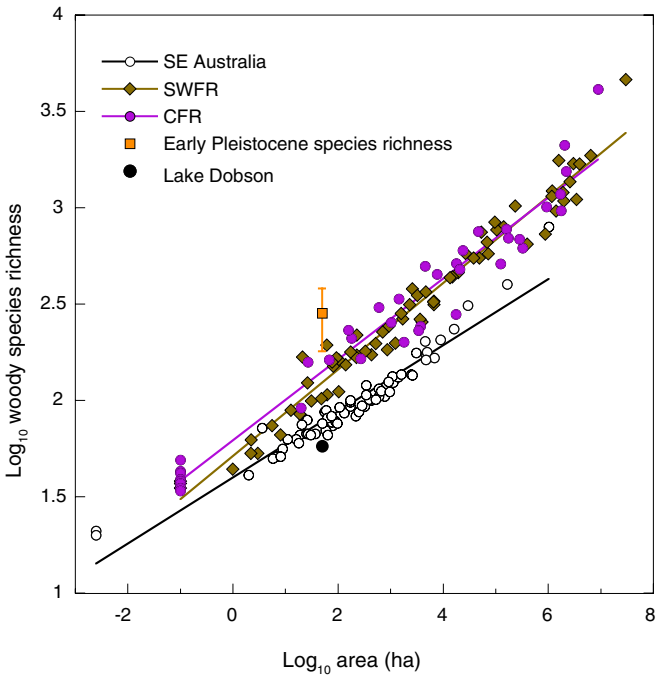

Fig. 3. Estimated woody sclerophyll species richness (288 species with 95% CI) in 50 ha vegetation during the Early Pleistocene in southeast Australia based on the SCB fossil flora. For comparison, woody species richness as a function of sampling area is shown for southeast Australia, the SWFR, and the CFR. Trend lines represent ordinary least squares regressions for the three regions (southeast Australia: $y = 1.5981 + 0.1716x$; SWFR: $y = 1.7101 + 0.2243x$; CFR: $y = 1.7915 + 0.2099x$). Also shown is woody sclerophyll species richness in the 50 ha catchment of LD, Tasmania.

predicted for SWFR ($P = 0.220$) and CFR ($P = 0.493$) (Table S3). The species/area relationships also confirmed that both CFR and SWFR have much higher woody plant diversities than southeast Australia at all spatial scales sampled ($P < 0.01$) (11) (Fig. 3 and *SI Text*). Although CFR [≥9,030 species (39)] has higher total plant species richness than SWFR [>7,380 species (5)], reflecting its much richer succulent and herbaceous component, their patterns of woody species richness are similar.

We evaluated the sensitivity of our species richness estimate to violations of our major assumptions. First, we considered the assumption that SCB and LD showed the same ratio of leaf assemblage to source vegetation species richness. The ratio observed at LD (0.314) is similar to comparable ratios observed in a New Zealand lake (mean = 0.377) (Table S2), despite large differences in leaf sclerophylly between the local floras. Even with an implausibly high ratio of one, the richness estimate for SCB source vegetation is considerably greater than the richest extant sclerophyll floras in southeast Australia, whereas any ratio ≤ 0.68 is consistent with Early Pleistocene SCB richness equaling the species richness of SWFR today. Second, the influence of underestimating catchment size at SCB should have been minor. The area of extant SWFR vegetation predicted to contain 288 woody species is 1,947 ha, ~39 times larger than our estimate of the source catchment size. More than a threefold error in estimating the catchment would require long-distance transport of plant fossils from outside of the hydrological catchment of SCB (40, 41).

Discussion

Our data are consistent with SCB having source vegetation at least as rich in woody species as SWFR or CFR on an equal area basis (Fig. 3). This inference holds even allowing for potential violations of our assumptions, such as exceptionally high representation of the surrounding vegetation in the fossil flora. Hence, the Early Pleistocene source vegetation was much richer in sclerophyll species than any vegetation in eastern Australia today. The regional mass extinction implicit in these results has passed largely unobserved, because many species in extant diverse sclerophyll floras share the same pollen types. Macrofossil records from Tasmania and southeast Australia have hinted at the scale of late Cenozoic plant species extinctions and imply that extinctions were largely complete by the middle Pleistocene (26, 42). However, the exceptional preservation of the SCB fossil flora uniquely allows discrimination between the morphologically convergent forms that characterize sclerophyll floras.

Our results show that, during the Early Pleistocene, southern Australia supported a hyperdiverse sclerophyll flora in a high-rainfall, summer-wet climate. These results undermine the notion that summer-dry Mediterranean-type climates are necessary for the evolution of hyperdiverse sclerophyll floras and demand a new model for the origins of sclerophyll diversity. A robust model must explain why diversity in the pyrophilic sclerophyll biome decreased in southeast Australia at the same time that mesic, pyrophobic rainforests across Australia declined in area and diversity (20, 21), although that decline has generally been attributed to cooler, drier, and more fire-prone conditions that may have favored sclerophyll vegetation. In addition, such a model should explain the existence of sclerophyll-dominated vegetation in non-Mediterranean climate regions with high rainfall, such as western Tasmania (43), parts of eastern Australia (44), and New Caledonia (45). We propose that the glacial–interglacial climate cycles in the Pleistocene depleted the diversity of both sclerophyll and rainforest communities in southeastern Australia. This explanation is consistent with the model of Jansson and Dynesius (46) that, in regions where Pleistocene glacial–interglacial cycles imposed high-amplitude changes in multiple aspects of the environment, specialist species were systematically and repeatedly extirpated, leaving less speciose floras dominated by generalists.

Why would these changes result in low diversity in eastern Australia but not in SWFR? The glacial–interglacial climate cycles of the Pleistocene may have had less impact on plants in southwest Australia than southeast Australia. Thus, pollen evidence suggests that shrublands persisted through the last glacial maximum (*ca*. 21 ka) in SWFR (47), whereas most of the forested southeast became steppe or grassland (21). These zonally contrasting responses are consistent with climate reconstructions for the last glacial maximum. Coupled ocean–atmosphere climate simulations indicate that winter precipitation increased in southwest Australia but decreased in the southeast (48), and offshore sea surface temperature reconstructions indicate smaller temperature depressions in southwest Australia than southeast Australia (49). Similarly, the modern west–east species richness gradient within CFR has been interpreted as resulting from lower-amplitude Pleistocene climate cycles in the west than the east (11).

Our results support the notion that sclerophyll plant hyperdiversity can, given enough time and environmental stability, develop outside Mediterranean-type climatic regimes. The current species richness of CFR and SWFR is, thus, primarily a product of their relatively stable Pleistocene climates and not a consequence of their shared summer-dry climates. Equivalently rich sclerophyll floras in southeast Australia under late Neogene summer-wet climate regimes were depleted, because fewer species were capable of tolerating the intensified climate cycles that developed later in the Pleistocene. Hence, the SWFR and CFR floras seem anomalously species-rich today, because few extratropical regions have experienced histories of low glacial–interglacial climate variability.

The previously cryptic extinction event shown here may not be restricted to the eastern Australian sclerophyll biome, because the methodological problems that lead to the delayed detection of this extinction event apply widely. Thus, fossil pollen has low taxonomic resolution everywhere, meaning that extinctions will be

invisible in this record if even one member of each pollen group survives. Although the current work shows that macrofossils can sometimes detect extinctions that are cryptic in the fossil pollen record, suitable Early Pleistocene macrofossil records are very rare worldwide. Most importantly, the proposed mechanism for these extinctions is not specific to the eastern Australian sclerophyll biome—although different regions experienced specific patterns of Pleistocene climate change, many extratropical regions were exposed to relatively high-amplitude Pleistocene climate changes. Thus, current biogeographic patterns may be more pervasively shaped by Pleistocene extinction than previously suspected, and similar patterns of extinction may extend to biomes—such as open, sclerophyllous, partly drought-adapted biomes—widely regarded as fully adapted to Late Quaternary climate regimes.

Materials and Methods

Study Site. SCB [37.35°S, 144.13°E, 550 m above sea level (asl)] (Fig. 1) is a small (<10 ha) paleolake within a small closed catchment in upland southeast Australia deposited over *ca*. 280 kya during the Early Pleistocene between 1.83 and 1.55 Ma (40). The paleolake infill consists of *ca*. 40 m organic-rich, silty clay sediments that contain exceptionally well-preserved fossil pollen, plant macrofossils (leaves, stems, flowers, and fruits) (Fig. 2), and insects. Previous analyses indicate that the vegetation was a mosaic of diverse sclerophyll forest and temperate rainforest (26, 41), with dynamics mediated, in part, by fire (50). Modern precipitation at SCB is dominated by cool-season frontal rain associated with seasonal migration of the subtropical anticyclone (51). However, fossil beetle-based climate reconstructions indicate much higher annual and summer precipitation during the Early Pleistocene (25), consistent with the presence in the record of a diverse conifer/angiosperm rainforest, including the highly drought-sensitive genera of Podocarpaceae (41, 52).

To provide a modern analog to SCB, we examined leaf assemblages from LD (42.67°S, 146.83°E, 1,030 m asl) (Fig. 1), a small (*ca*. 3 ha) cirque lake in Mount Field National Park, Tasmania, Australia, with a hydrological catchment of *ca*. 60 ha. Intensive field sampling identified 58 woody angiosperm species in the catchment.

Fossil Sampling and Identification. We analyzed plant macrofossils from four stratigraphically sequential 3,000-mL sediment samples of 10 cm stratigraphic thickness taken between 470 and 500 cm deep in an excavation near the center of SCB. These samples were chosen, because they contained numerous macrofossils—other samples appeared to show comparable diversity to those samples analyzed but contained too few macrofossils for analysis. Pollen analyses indicate that the four samples are equivalent to the *Eucalyptus*-dominated Zone A of the pollen record of Sniderman and Haberle (50). We estimate that each sample represents *ca*. 635 y of deposition based on the age model of Sniderman and Haberle (50).

Estimation of Early Pleistocene Standing Diversity. We estimated the species richness of the Early Pleistocene source vegetation around SCB by (*i*) estimating the asymptotic richness of the SCB fossil flora, (*ii*) quantitatively examining the relationship between the richness of extant sclerophyll vegetation and its representation in lacustrine leaf assemblages on the basis of equal sampling effort, and (*iii*) evaluating the extent to which the observed richness of the SCB fossil flora may have been positively biased by time averaging. Finally, to evaluate the evolutionary and ecological significance of the Early Pleistocene sclerophyll vegetation represented at SCB, we compared the estimated richness of the SCB source vegetation with the richest extant sclerophyll vegetation in Australia and the CFR on an equal area basis (*SI Text*). We compiled separate species/area curves for southeast and southwest Australia and CFR, and we used linear models to compare their slopes and intercepts of regressions of $\log_{10}$ of species richness with $\log_{10}$ of area (*SI Text*, Figs. S1–S2, Tables S1–S5).

ACKNOWLEDGMENTS. We thank the Center for Nanoscale Systems (Harvard University), particularly Richard Schalek; the Central Science Laboratory (University of Tasmania), particularly Karsten Goemann; Kate Bromfield and Liam Mulcahy for some of the scanning EM; Josephine Brown for help with Fig. 1; and Malte Meinshausen for help with Monte Carlo simulations. For discussions and comments on the manuscript, we thank Malte Meinshausen, Matt McGlone, and Peter Wilf. This work was partly supported by a Bullard Fellowship (Harvard University) and Australian Research Council Grants DE120102530 (to J.M.K.S.), DP110104926 (to G.J.J.), and DP0878342 (to G.J.J.).

1. Cowling RM, Rundel PW, Lamont BB, Kalin Arroyo M, Arianoutsou M (1996) Plant diversity in Mediterranean-climate regions. *Trends Ecol Evol* 11(9):362–366.
2. Kreft H, Jetz W (2007) Global patterns and determinants of vascular plant diversity. *Proc Natl Acad Sci USA* 104(14):5925–5930.
3. Currie DJ, et al. (2004) Predictions and tests of climate-based hypotheses of broad-scale variation in taxonomic richness. *Ecol Lett* 7(12):1121–1134.
4. Wiens JJ, Donoghue MJ (2004) Historical biogeography, ecology and species richness. *Trends Ecol Evol* 19(12):639–644.
5. Hopper SD, Gioia P (2004) The southwest Australian floristic region: Evolution and conservation of a global hot spot of biodiversity. *Annu Rev Ecol Evol Syst* 35:623–650.
6. Cowling RM, Procheş S, Partridge TC (2009) Explaining the uniqueness of the Cape flora: Incorporating geomorphic evolution as a factor for explaining its diversification. *Mol Phylogenet Evol* 51(1):64–74.
7. Wright IJ, et al. (2004) The worldwide leaf economics spectrum. *Nature* 428(6985): 821–827.
8. Lambers H, Brundrett MC, Raven JA, Hopper SD (2010) Plant mineral nutrition in ancient landscapes: High plant species diversity on infertile soils is linked to functional diversity for nutritional strategies. *Plant Soil* 334(1–2):11–31.
9. Hopper SD (2009) OCBIL theory: Towards an integrated understanding of the evolution, ecology and conservation of biodiversity on old, climatically buffered, infertile landscapes. *Plant Soil* 322(1–2):49–86.
10. Linder HP (2003) The radiation of the Cape flora, southern Africa. *Biol Rev Camb Philos Soc* 78(4):597–638.
11. Cowling RM, Lombard AT (2002) Heterogeneity, speciation/extinction history and climate: Explaining regional plant diversity patterns in the Cape Floristic Region. *Divers Distrib* 8(3):163–179.
12. Fox MD (1994) Australian Mediterranean vegetation: Intra- and intercontinental comparisons. *Ecology and Biogeography of Mediterranean Ecosystems of Chile*, eds Arroyo MTK, Fox MD, Zedler PH (Springer, New York), pp 137–159.
13. Hopper SD (1992) Patterns of diversity at the population and species levels in southwest Australian Mediterranean ecosystems. *Biodiversity of Mediterranean Ecosystems in Australia*, ed Hobbs RJ (Surrey Beattey & Sons, Sydney), pp 27–46.
14. Goldblatt P, Manning JC (2002) Plant diversity of the Cape Region of southern Africa. *Ann Mo Bot Gard* 89(2):281–302.
15. Linder HP (2008) Plant species radiations: Where, when, why? *Philos Trans R Soc Lond B Biol Sci* 363(1506):3097–3105.
16. Schnitzler J, et al. (2011) Causes of plant diversification in the Cape biodiversity hotspot of South Africa. *Syst Biol* 60(3):343–357.
17. Jordan GJ, Hill RS (1996) The fossil record of the Epacridaceae. *Ann Bot* 77(4):341–346.
18. Crisp MD, Burrows GE, Cook LG, Thornhill AH, Bowman D (2011) Flammable biomes dominated by eucalypts originated at the Cretaceous-Palaeogene boundary. *Nat Commun* 2:193, 10.1038/ncomms1191.
19. Crisp MD, Cook L, Steane D (2004) Radiation of the Australian flora: What can comparisons of molecular phylogenies across multiple taxa tell us about the evolution of diversity in present-day communities? *Philos Trans R Soc Lond B Biol Sci* 359(1450): 1551–1571.
20. Kershaw AP, Martin HA, McEwan Mason JRC (1994) The Neogene: A period of transition. *History of the Australian Vegetation: Cretaceous to Recent*, ed Hill RS (Cambridge Univ Press, Cambridge, United Kingdom), pp 299–327.
21. Kershaw AP, D'Costa DM, McEwan Mason JRC, Wagstaff BE (1991) Palynological evidence for Quaternary vegetation and environments of mainland southeastern Australia. *Quat Sci Rev* 10(5):391–404.
22. Linder HP, Meadows M, Cowling RM (1992) History of the Cape flora. *The Ecology of Fynbos: Nutrients, Fire and Diversity*, ed Cowling RM (Oxford Univ Press, London), pp 113–134.
23. Martin HA (1994) Australian Tertiary phyogeography: Evidence from palynology. *History of the Australian Vegetation: Cretaceous to Recent*, ed Hill RS (Cambridge Univ Press, Cambridge, United Kingdom), pp 104–142.
24. Birks HH (2007) Plant macrofossil introduction. *Encyclopedia of Quaternary Science* (Elsevier, Amsterdam) ed Scott A, Vol 3, pp 2266–2288.
25. Sniderman JMK, Porch N, Kershaw AP (2009) Quantitative reconstruction of Early Pleistocene climate in southeastern Australia and implications for atmospheric circulation. *Quat Sci Rev* 28(27,28):3185–3196.
26. Jordan GJ, Bromfield KE, Sniderman JMK, Crayn D (2007) Diverse fossil epacrids (Styphelioideae; Ericaceae) from Early Pleistocene sediments at Stony Creek Basin, Victoria, Australia. *Int J Plant Sci* 168(9):1359–1376.
27. Carpenter RJ, Hill RS, Jordan GJ (2005) Leaf cuticular morphology links Platanaceae and Proteaceae. *Int J Plant Sci* 166(5):843–855.
28. Watson L (1967) Taxonomic implications of a comparative anatomical study of Epacridaceae. *New Phytol* 66(3):495–504.
29. Jordan GJ, Dillon RA, Weston PH (2005) Solar radiation as a factor in the evolution of scleromorphic leaf anatomy in Proteaceae. *Am J Bot* 92(5):789–796.
30. Hill RS, Gibson N (1986) Distribution of potential macrofossils in Lake Dobson, Tasmania. *J Ecol* 74(2):373–384.
31. Spicer RA (1989) The formation and interpretation of plant fossil assemblages. *Adv Bot Res* 16:95–191.
32. Wing SL, DiMichele WA (1995) Conflict between local and global changes in plant diversity through geological time. *Palaios* 10(6):551–564.
33. Wilf P, et al. (2003) High plant diversity in Eocene South America: Evidence from Patagonia. *Science* 300(5616):122–125.

34. Burnham RJ (1993) Reconstructing richness in the plant fossil record. *Palaios* 8(4): 376–384.
35. Burnham RJ (1994) Paleoecological and floristic heterogeneity in the plant-fossil record: An analysis based on the Eocene of Washington. *US Geol Surv Bull* 2085-B:1–36.
36. Jost L (2007) Partitioning diversity into independent alpha and beta components. *Ecology* 88(10):2427–2439.
37. Veech JA, Summerville KS, Crist TO, Gering JC (2002) The additive partitioning of species diversity: Recent revival of an old idea. *Oikos* 99(1):3–9.
38. Chao A, Lee S-M (1992) Estimating the number of classes via sample coverage. *J Am Stat Assoc* 87(417):210–217.
39. Goldblatt P, Manning JC (2000) Cape plants: A conspectus of the Cape Flora of South Africa. *Pretoria, South Africa: National Botanical Institute* 9:1–744.
40. Sniderman JMK, Pillans B, O'Sullivan PB, Kershaw AP (2007) Climate and vegetation in southeastern Australia respond to southern hemisphere insolation forcing in the late Pliocene-early Pleistocene. *Geology* 35(1):41–44.
41. Sniderman JMK (2011) Early Pleistocene vegetation change in upland south-eastern Australia. *J Biogeogr* 38(8):1456–1470.
42. Jordan GJ (1997) Evidence of Pleistocene plant extinction and diversity from Regatta Point, western Tasmania, Australia. *Bot J Linn Soc* 123(1):45–71.
43. Reid JB, Hill R, Hovenden MJ, eds (1999) *Vegetation of Tasmania* (Australian Biological Resources Study, Canberra, Australia).
44. Specht RL (1994) Heathlands. *Australian Vegetation*, ed Groves RH (Cambridge Univ Press, Cambridge, United Kingdom), pp 321–344.
45. Read J, Sanson GD, Garine-Wichatitsky Md, Jaffré T (2006) Sclerophylly in two contrasting tropical environments: Low nutrients vs. low rainfall. *Am J Bot* 93(11): 1601–1614.
46. Jansson R, Dynesius M (2002) The fate of clades in a world of recurrent climatic change: Milankovitch oscillations and evolution. *Annu Rev Ecol Syst* 33:741–777.
47. Dodson JR (2001) Holocene vegetation change in the Mediterranean-type climate regions of Australia. *Holocene* 11(6):673–680.
48. Rojas M, et al. (2009) The Southern Westerlies during the last glacial maximum in PMIP2 simulations. *Clim Dyn* 32(4):525–548.
49. Barrows TT, Juggins S (2005) Sea-surface temperatures around the Australian margin and Indian Ocean during the Last Glacial Maximum. *Quat Sci Rev* 24(7–9):1017–1047.
50. Sniderman JMK, Haberle SG (2012) Fire and vegetation change during the Early Pleistocene in southeastern Australia. *J Quat Sci* 27(3):307–317.
51. Hobbs JE (1999) Present climates of Australia and New Zealand. *Climate of the Southern Continents: Present, Past and Future*, eds Hobbs JE, Lindesay JA, Bridgman HA (Wiley, New York), pp 63–105.
52. Brodribb T, Hill R (2004) The rise and fall of Podocarpaceae in Australia—a physiological explanation. *The Evolution of Plant Physiology*, eds Hemsley AR, Poole I (Elsevier, London), pp 381–399.

Supporting Information Appendix

Supplementary Figures S1-S35

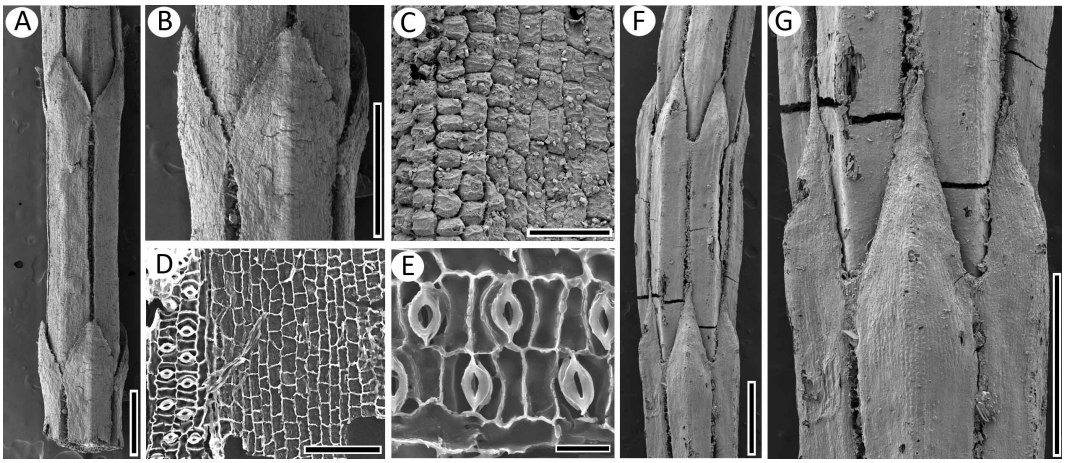

Fig. S1. Scanning electron micrographs of Casuarinaceae species from Stony Creek Basin. **A.** Photosynthetic stem of *Allocasuarina* cf. *torulosa*. Scale bar = 0.5 mm. **B**. Detail showing teeth and groove running down the stem. The stomata are encrypted in the groove. Scale bar = 0.5 mm. **C.** Detail of eroded stem surface showing the epidermal cell shapes. The shorter cells are along the ridge. Scale bar = 50 µm. **D.** Inner surface of a prepared cuticle from an organically preserved (non-carbonized) specimen. Note the stomata arrayed in 2 lines, and oriented at right angles to the stem. Scale bar = 100 µm. **E.** Detail of a prepared cuticle showing the stomatal morphology typical of Casuarinaceae. Scale bar = 10 µm. **F.** Photosynthetic stem of *Allocasuarina* species 2. This species differs from *A.* cf. *torulosa* in having 6-7 teeth (rather than 4 or rarely 5), and much longer teeth that are attenuate. These characters are considered significant for separating extant species (1). Scale bar = 0.5 mm. **G**. Photosynthetic stem of *Allocasuarina* species 2, showing the teeth and groove containing stomata. Scale bar = 0.5 mm.

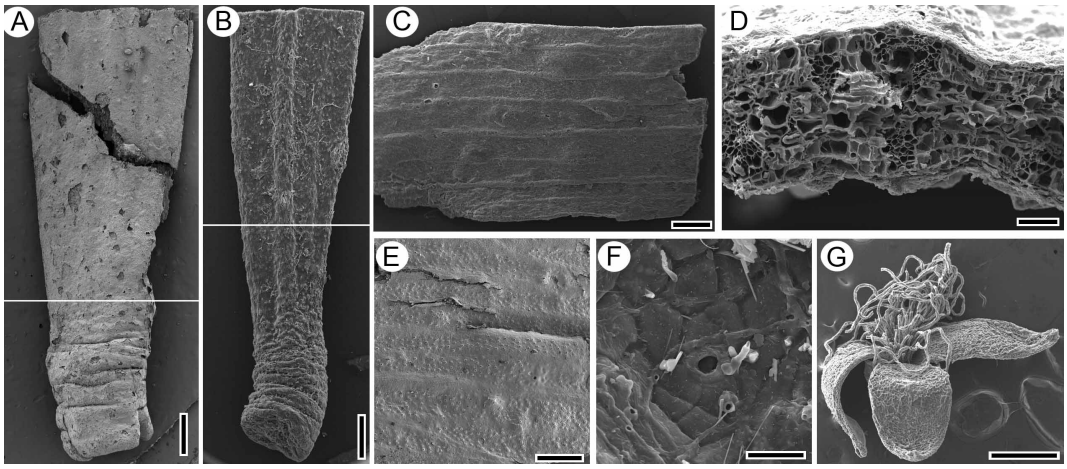

Fig. S2. Scanning electron micrographs of *Acacia* (Fabaceae: Mimosoideae) species from Stony Creek Basin. **A - C.** Phyllode fragments of *Acacia* species. Scale bar = 0.5mm. **D.** Transverse section of *Acacia* species 1. Scale bar = 50 µm. **E.** Surface detail of *Acacia* species 1 showing stomatal distribution. Scale bar = 0.5mm. **F.** Surface detail of *Acacia* species 1 showing a stoma and mesophyll cells. Scale bar = 20 µm. **G.** Flower of undetermined species of *Acacia*. Scale bar = 0.5mm.

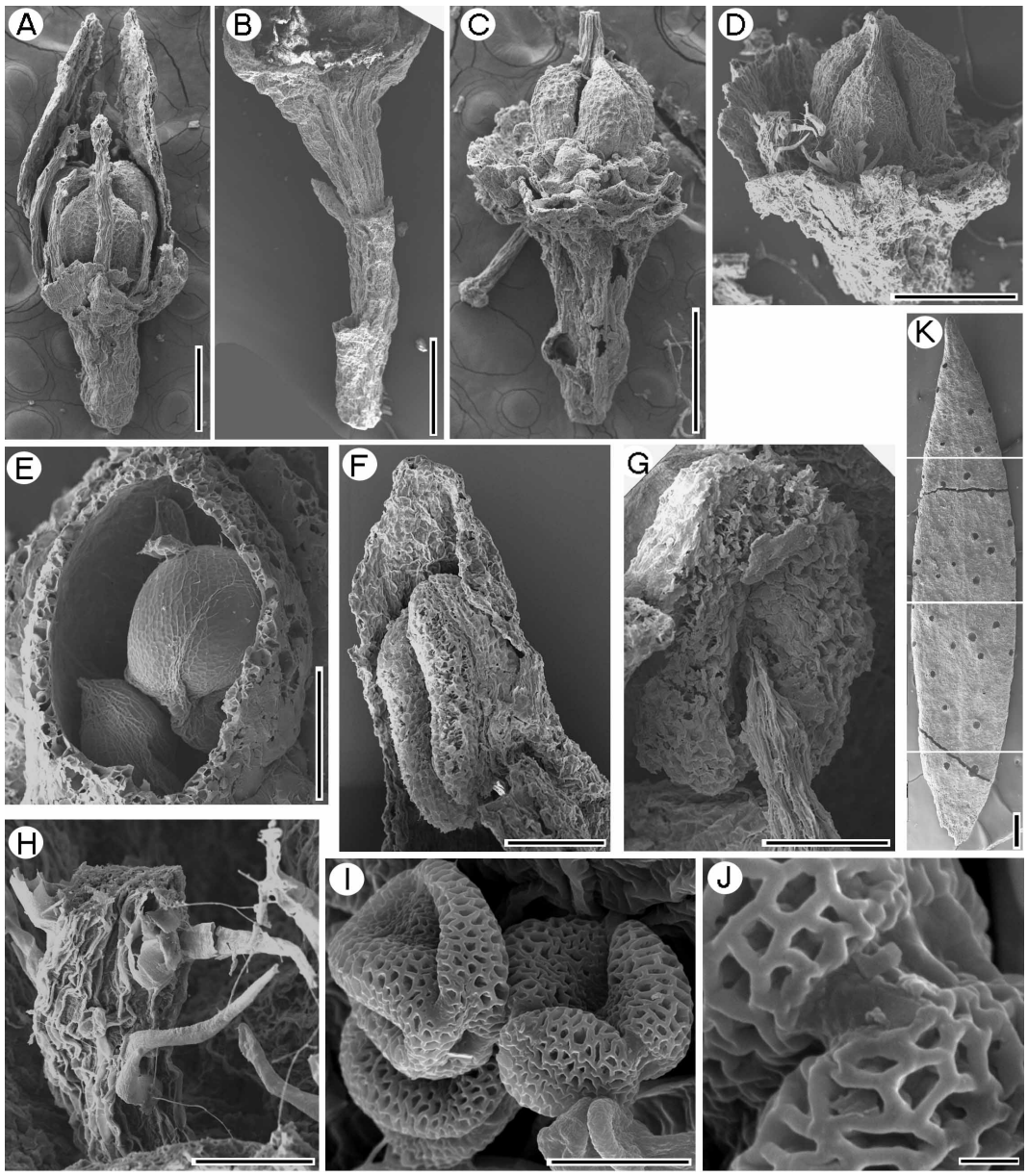

Fig. S3. Scanning electron micrographs of flowers of *Boronia* cf. *parvifolia* (Rutaceae) flowers and possible *Boronia* leaf from Stony Creek Basin. **A.** *Boronia* flower with intact components. Note the petals, ovaries and stigma. Scale bar = 0.5 mm. **B.** *Boronia* flower peduncle. Scale bar = 0.5 mm. **C.** *Boronia* flower. Note the visible ovaries. Scale bar = 0.5 mm. **D.** *Boronia* flower. Note the visible ovaries. Scale bar = 0.5 mm. **E.** Detail of single ovary and seeds. Scale bar = 200 μm. **F.** Detail of anther. Scale bar = 200 μm. **G.** Detail of anther. Note the attachment of filament. Scale bar = 100 μm. **H.** Detail of anther filament. Note the hairs. Scale bar = 100 μm. **I.** *Boronia* pollen *in situ* in the anther. Scale bar = 10 μm. **J.** Detail of *Boronia* pollen showing exine sculpturing. Scale bar = 1 μm. **K.** Possible leaf of *Boronia*. Note the conspicuous bulging oil glands. This leaf is broadly consistent with *Boronia* but could be of some related taxon. This is a composite image (as indicated by white lines). Scale bar = 0.5 mm.

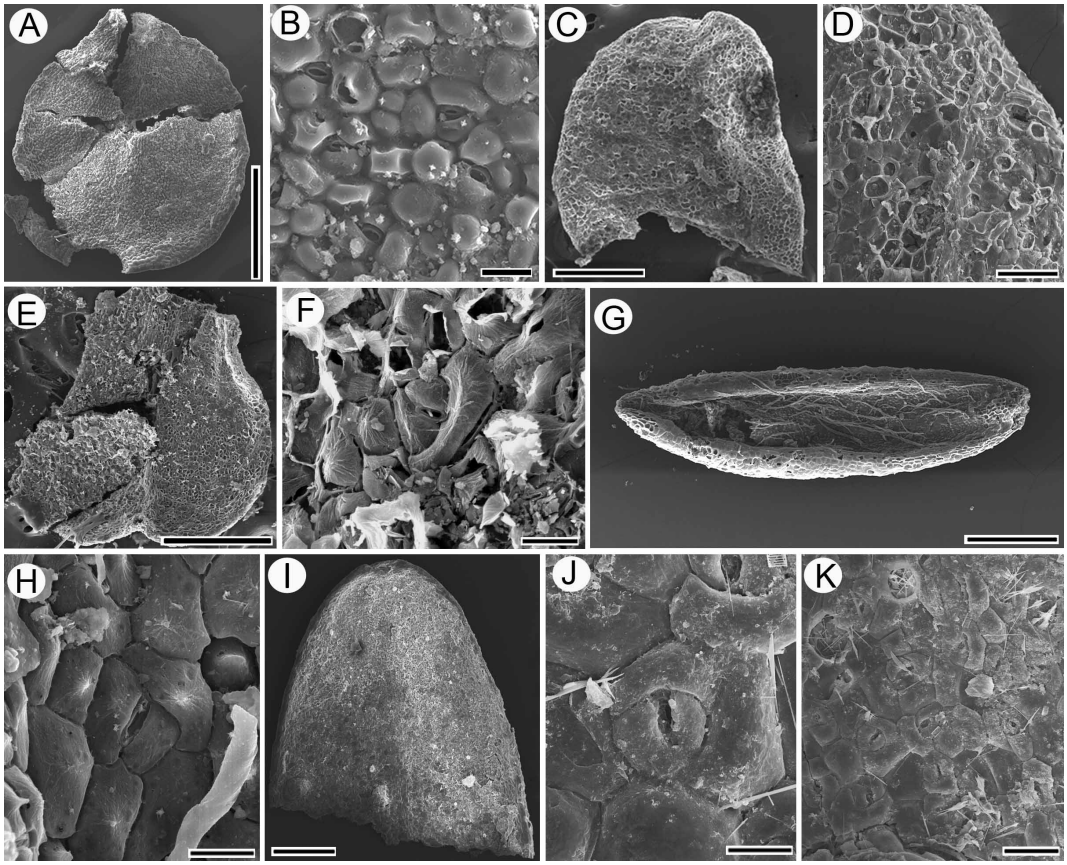

Fig. S4. Scanning electron micrographs of Fabaceae subfamily Faboideae species from Stony Creek Basin. **A, C, E**. Leaves of Fabaceae species 1. This species is consistent with some modern Australian sclerophyll genera within tribe Bossieae, including *Bossiaea* (see (2) for illustrations of the distinctive cuticles of this group). The key character is the anisocytic stomata combined with bulging epidermal cells (sometimes with the distinctive papillae apparent in **F**). Fabaceae species 2 and 3 also have these features Scale bars = 0.5 mm. **B.** Fabaceae species 1. Detail of epidermis of specimen shown in **A**. Note the anisocytic stomata and papillae. Scale bar = 20 μm. **D.** Fabaceae species 1. Detail of epidermis of specimen shown in **C**. Scale bar = 100 μm. **F.** Fabaceae species 1. Detail of epidermis of specimen shown in **E**. Note the stomata and papillae. Scale bar = 20 μm. **G.** Leaf of Fabaceae species 2. Scale bar = 0.5 mm. This species is consistent with the Australian sclerophyll genus *Aotus*. **H.** Fabaceae species 2. Detail of epidermis. Note the anisocytic stomata and papillae. Scale bar = 20 μm. **I.** Leaf of Fabaceae species 4. Scale bar = 0.5 mm. This species is consistent with a number of Australian sclerophyll genera. The leaf shape is quite distinct from the other Fabaceae described here. **J.** Fabaceae species 4. Detail of epidermis. Note the anisocytic stomata and bulging epidermal cells. Scale bar = 20 μm. **K.** Fabaceae species 4. Detail of epidermis. Note the randomly oriented stomata. Scale bar = 50 μm.

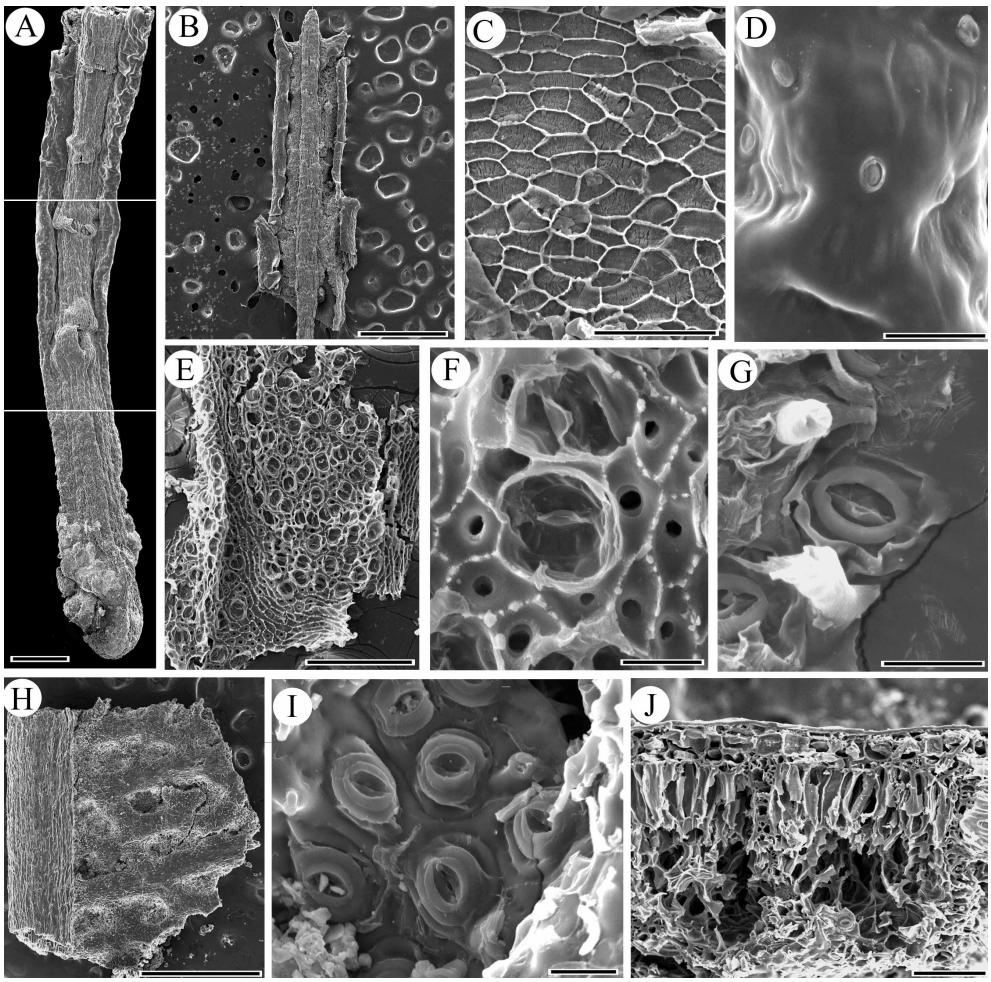

Fig. S5. Scanning electron micrographs of *Banksia* (Proteaceae) species from Stony Creek Basin. **A.** *B. ericifolia* leaf base. This is a composite image (as indicated by white lines). Scale bar = 500 µm. **B.** *B. ericifolia* whole leaf number 2. Scale bar = 1 mm. The three pointed leaf apex combined with the revolute margins is diagnostic for *B. ericifolia.* The stomatal morphology and trichome bases are also characteristic of *Banksia*. **C.** *B. ericifolia* lamina detail showing epidermal cells. Scale bar = 100 µm. **D.** *B. ericifolia* surface detail. Scale bar = 40 µm. **E.** *B. ericifolia* leaf surface showing stomata. Scale bar = 200 µm. **F.** *B. ericifolia* surface detail showing a stoma. Scale bar = 20 µm. **G.** *B.ericifolia* surface detail showing a stoma. Scale bar = 20 µm. **H.** *Banksia* cf. *marginata* lamina fragment. Scale bar = 1 mm. This species is clearly different from *B. ericifolia* because the stomata are restricted to areoles which are sunken beneath the leaf surface. This is a diagnostic character for major clades within *Banksia*. **I.** *Banksia* cf. *marginata* surface detail showing stomata. These are typical of *Banksia.* Scale bar = 20 µm. **J.** *Banksia* cf. *marginata* transverse section. This shows the characteristic anatomy of most *Banksia*, with bundle sheath extension and double hypodermis. Scale bar = 100 µm.

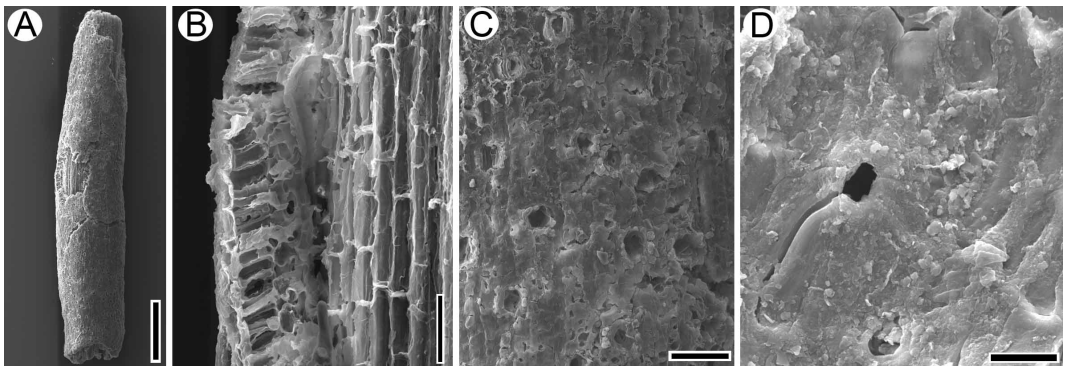

Fig. S6. Scanning electron micrographs of *Hakea* (Proteaceae) species from Stony Creek Basin. **A.** Leaf fragment. Scale bar = 0.5 mm. **B.** Broken edge, showing the tightly packed, well developed palisade parenchyma surrounding core of lignified cells (typical of *Hakea*). Scale bar = 20 µm. **C.** Outer leaf surface (variably degraded) showing deeply sunken stomata, aligned parallel to the long axis of the leaf. Scale bar = 50 µm. **D.** Outer leaf surface showing the cone-like ring of epidermal cells encrypting a stoma. This is characteristic of *Hakea*. Scale bar = 20 µm.

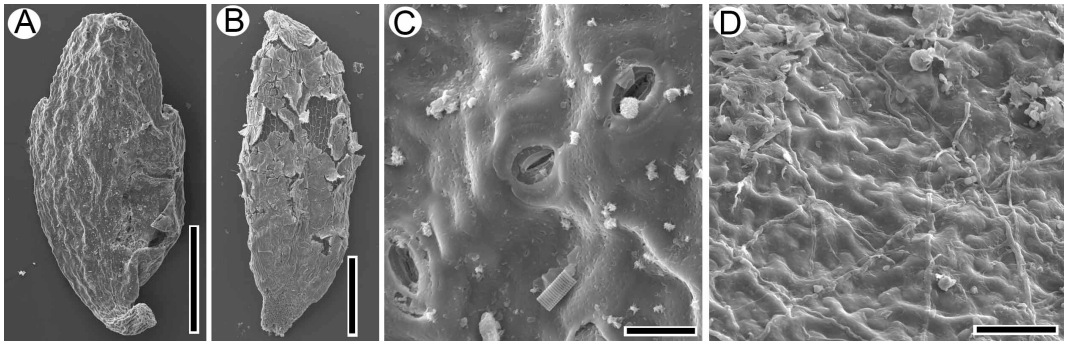

Fig. S7. Scanning electron micrographs of *Bauera* (Cunoniaceae) species from Stony Creek Basin. **A.** Leaf showing abaxial (lower) surface with stomata. Scale bar = 500 μm. **B.** Leaf showing adaxial (upper) surface with no stomata. Note the way that the epidermis detaches from the mesophyll. *Bauera* is very unusual in that the adaxial epidermis is separated from the mesophyll by a layer of mucilage. Scale bar = 0.5 mm. **C.** Abaxial leaf surface showing stomata. Scale bar = 20 μm. **D.** Adaxial leaf surface showing the outlines of epidermal cells with sinuous walls. Scale bar = 50 μm.

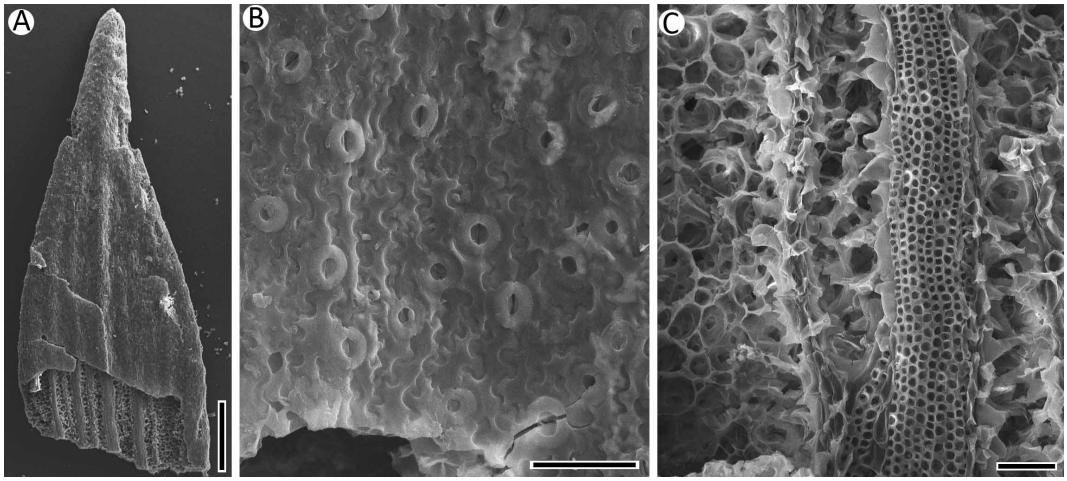

Fig. S8. Undescribed species of *Epacriphyllum* (Ericaceae subfamily Styphelioideae) from Stony Creek Basin. **A.** Leaf apex showing the thick (and presumably pungent) acuminate apex, and parallel veins. Scale bar = 0.5 mm. **B.** Detail of leaf surface showing stomata with axes aligned parallel to the main veins, and outlines of epidermal cells which are aligned parallel to the veins and have strongly sinuous cell walls. Scale bar = 50 μm. **C.** Detail of leaf anatomy showing a vein and mesophyll cells. Scale bar = 50 μm.

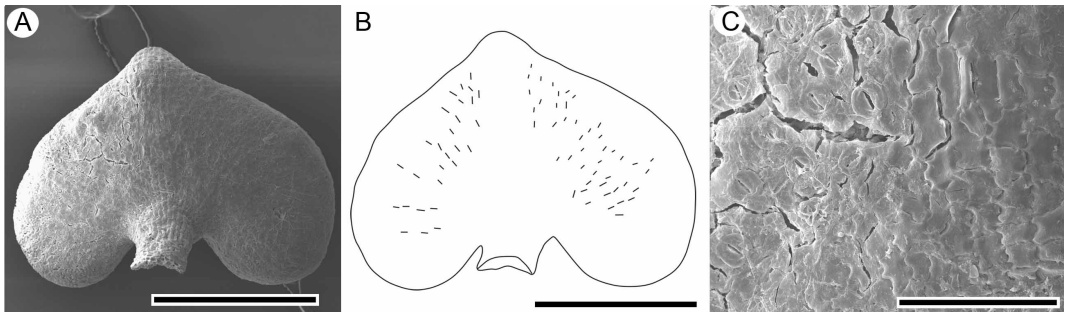

Fig. S9. Scanning electron micrographs and one line drawing of fossil leaves of *Epacriphyllum* species 1 (Ericaceae subfamily Styphelioideae) from Stony Creek Basin. Reproduced with permission from (3), with formatting slightly modified to make it consistent with other figures. **A.** Abaxial leaf surface. Scale bar = 0.5 mm. **B.** Line drawing of abaxial leaf surface showing position and alignment of stomata Scale bar = 0.5 mm. **C.** Detail of abaxial leaf surface showing stomata, and shape of epidermal cells. Scale bar = 100 μm.

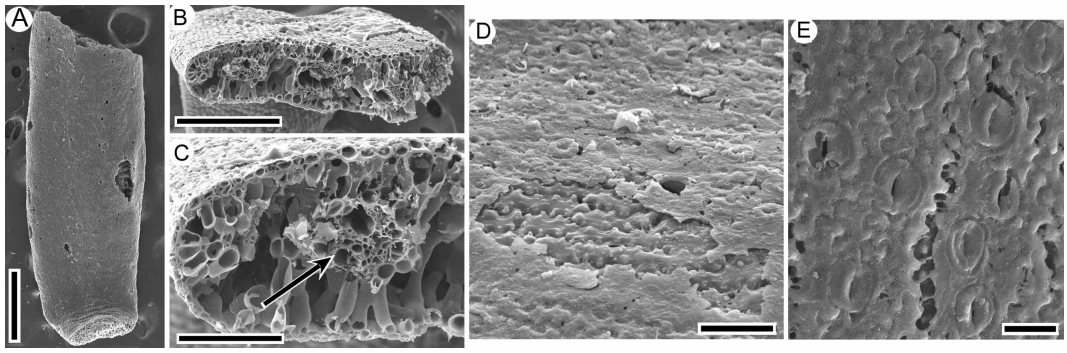

Fig. S10. Scanning electron micrographs of fossil leaves of *Epacriphyllum* species 2 (Ericaceae subfamily Styphelioideae) from Stony Creek Basin. Reproduced with permission from (3), with formatting slightly modified to make it consistent with other figures. **A**. Abaxial surface. Scale bar = 0.5 mm. **B.** Cross section. Scale bar = 300 μm. **C.** Cross section showing vascular bundle placed approximately midway between adaxial and abaxial surfaces (arrow). Scale bar = 100 μm. **D.** Abaxial leaf surface showing stomata and elongate epidermal cells with sinuous walls. Scale bar = 50 μm. **E.** Abaxial leaf surface showing stomata and sinuous cell walls. Scale bar = 20 μm.

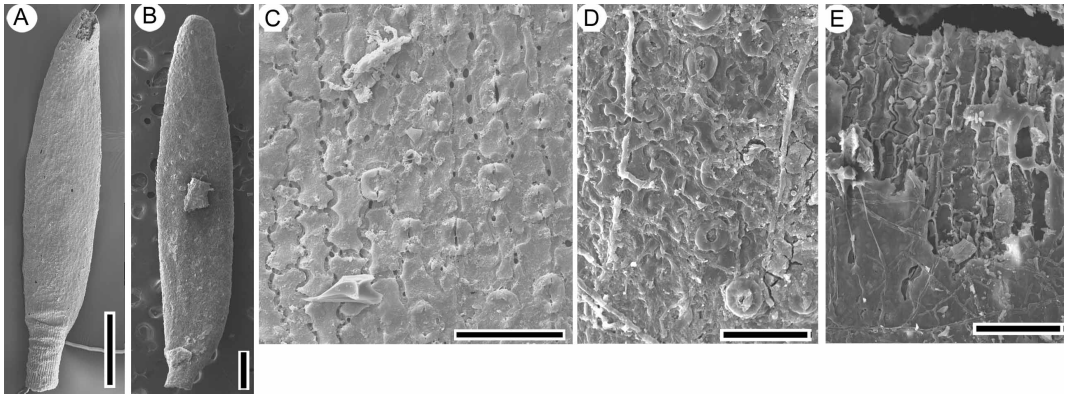

Fig. S11. Scanning electron micrographs of fossil leaves of *Epacriphyllum* species 3 (Ericaceae subfamily Styphelioideae) from Stony Creek Basin. Reproduced with permission from (3), with formatting slightly modified to make it consistent with other figures. **A, B.** Abaxial leaf surface of leaves. Scale bar = 0.5 mm. **C.** Abaxial leaf surface showing stomata and relatively short epidermal cells with sinuous walls. Scale bar = 50 μm. **D.** Abaxial leaf surface showing stomata and epidermal cells. Scale bar = 50 μm. **E.** Adaxial leaf surface showing elongate epidermal cells with sinuous walls. Scale bar = 100 μm.

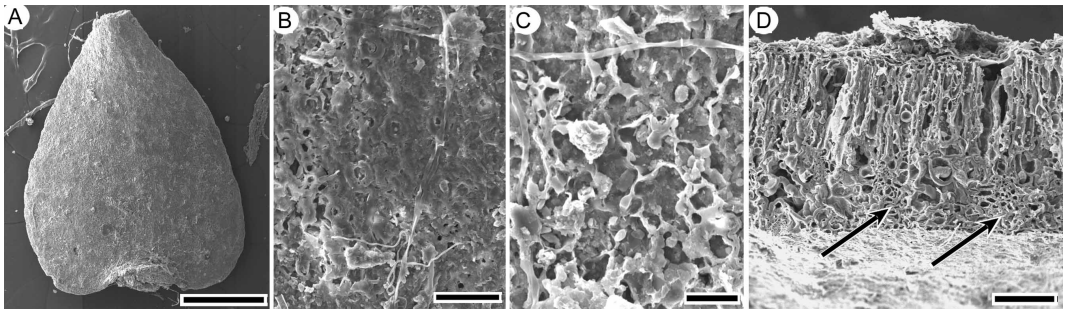

Fig. S12. Scanning electron micrographs of fossil leaves of *Epacriphyllum* species 4 (Ericaceae subfamily Styphelioideae) from Stony Creek Basin. Reproduced with permission from (3), with formatting slightly modified to make it consistent with other figures. **A.** Abaxial leaf surface. Scale bar = 1 mm. **B.** Detail of abaxial leaf surface showing stomata, and shape of epidermal cells. Scale bar = 50 μm. **C.** Detail of eroded abaxial leaf surface showing the sinuous cell walls of the epidermal cells of veinal region. Scale bar = 20 μm. **D.** Cross section of lamina. Note that there has been artefactual thickening of the cell walls of some tissues. Scale bar = 100 μm.

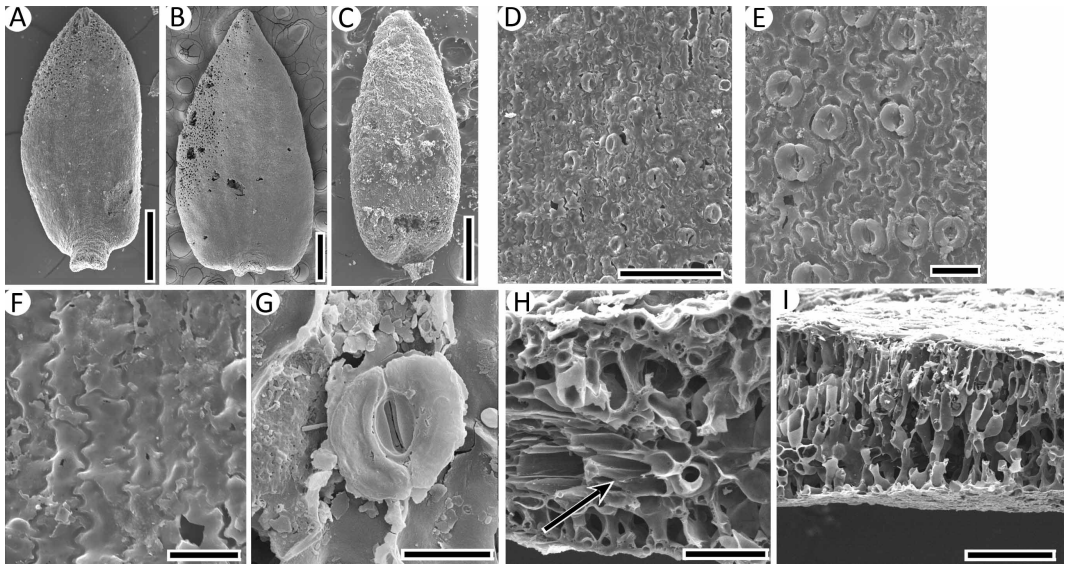

Fig. S13. Scanning electron micrographs of fossil leaves of *Epacriphyllum* species 5 (Ericaceae subfamily Styphelioideae) from Stony Creek Basin. Reproduced with permission from (3), with formatting slightly modified to make it consistent with other figures. **A-C.** Abaxial surface of leaves. Scale bar = 0.5 mm. **D.** Partially eroded abaxial leaf surface showing stomata and epidermal cells. Scale bar = 100 μm. **E.** Partially eroded abaxial leaf surface showing stomata and short epidermal cells with sinuous walls. Scale bar = 20 μm. **F.** Adaxial leaf surface showing short epidermal cells with sinuous walls. Scale bar = 20 μm. **G.** Eroded adaxial leaf surface showing a stoma. Scale bar = 10 μm. **H.** Cross section showing a vascular bundle (arrow) with mesophyll tissue above and below it. Note also the small epidermal cells. Scale bar = 50 μm. **I.** Cross section showing mesophyll tissue. Scale bar = 100 μm.

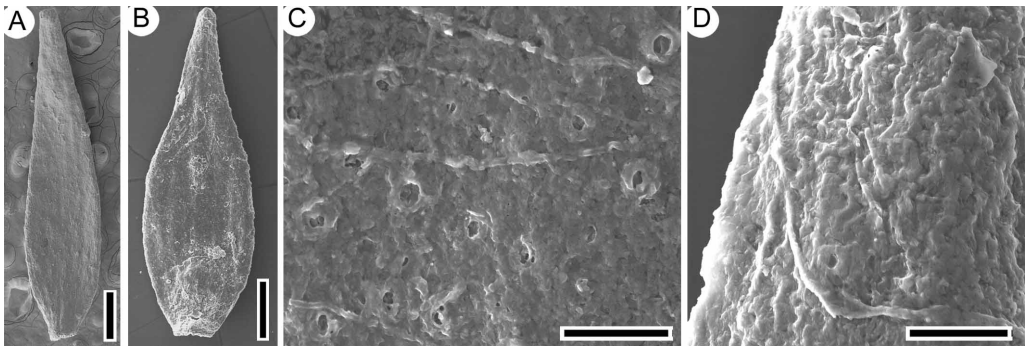

Fig. S14. Scanning electron micrographs of fossil leaves of *Epacriphyllum* species 6 (Ericaceae subfamily Styphelioideae) from Stony Creek Basin. Reproduced with permission from (3), with formatting slightly modified to make it consistent with other figures. **A, B.** Abaxial surface of leaves. Scale bars = 0.5 mm. **C.** Abaxial leaf surface showing stomata. Scale bar = 50 μm. **D.** Abaxial leaf surface showing sinuous epidermal cell walls. Scale bar = 50 μm.

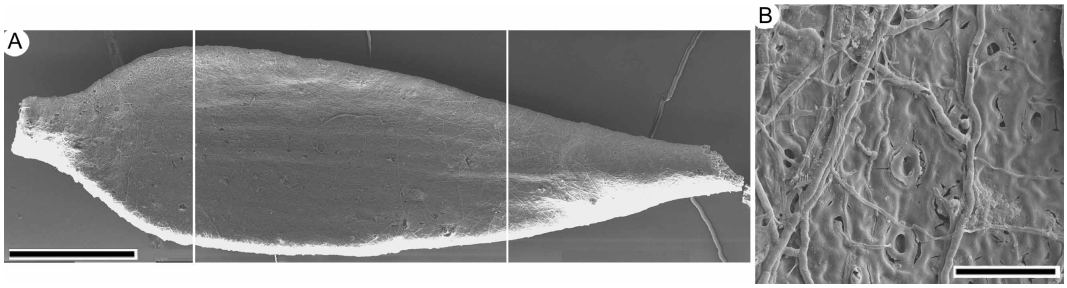

Fig. S15. Scanning electron micrographs of fossil leaves of *Epacriphyllum* species 7 (Ericaceae subfamily Styphelioideae) from Stony Creek Basin. Reproduced with permission from (3), with formatting slightly modified to make it consistent with other figures. **A.** Abaxial leaf surface. Scale bar = 1 mm. This is a composite image (as indicated by white lines). **B.** Abaxial leaf surface of showing stomata aligned with the midrib and indications of the presence of sinuous cell walls. Scale bar = 50 μm.

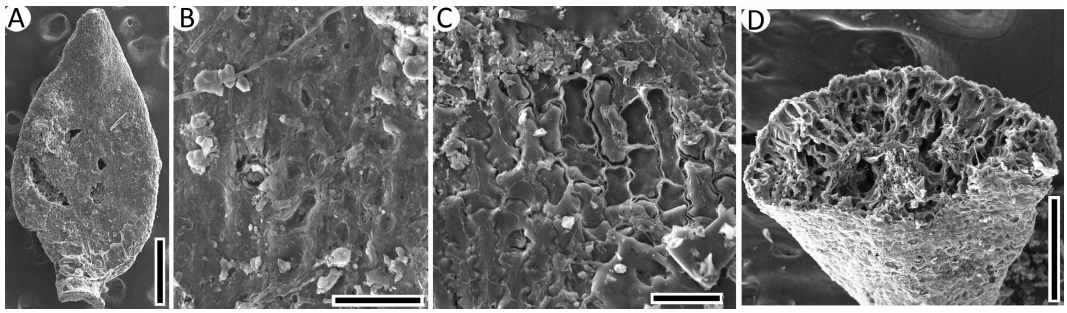

Fig. S16. Scanning electron micrographs of fossil leaves of *Epacriphyllum* species 8 (Ericaceae subfamily Styphelioideae) from Stony Creek Basin. Reproduced with permission from (3), with formatting slightly modified to make it consistent with other figures. **A.** Abaxial leaf surface. Scale bar = 0.5 mm. **B.** Abaxial leaf surface showing stomata. Scale bar = 50 μm. **C.** Partially eroded adaxial leaf surface showing short, sinuous-walled epidermal cells. Scale bar = 50 μm. **D.** Cross section of leaf showing distribution of mesophyll cells and vascular bundles. Scale bar = 200 μm.

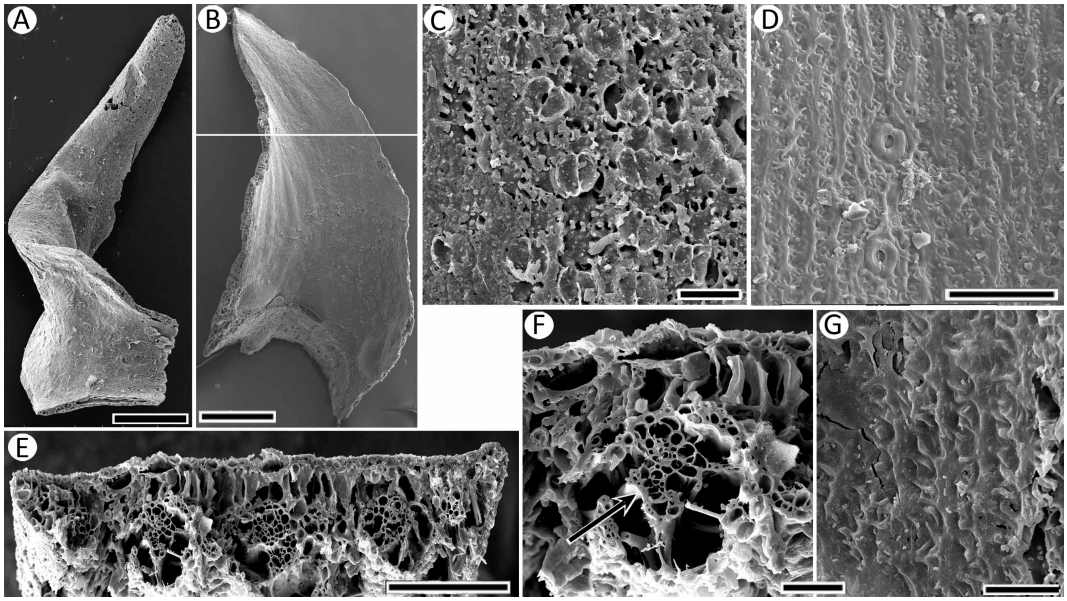

Fig. S17. Scanning electron micrographs of fossil leaves of Cosmelieae sp. (Ericaceae subfamily Styphelioideae) from Stony Creek Basin. Reproduced with permission from (3), with formatting slightly modified to make it consistent with other figures. **A.** Abaxial leaf surface. Scale bar = 0.5 mm. The lateral parts of the leaf base have been broken off. **B.** Abaxial leaf surface. Scale bar = 0.5 mm. This is a composite image (as indicated by white line). **C.** Partially eroded abaxial leaf surface showing stomata and sinuous cell walls. Scale bar = 50 μm. **D.** Abaxial leaf surface showing cyclocytic stomata and sinuous-walled epidermal cells. Scale bar = 50 μm. **E.** Cross section of leaf showing several vascular bundles adjacent to the adaxial surface. Scale bar = 100 μm. **F.** Cross section of leaf showing a vascular bundle adjacent to the adaxial surface and separated from the abaxial surface by mesophyll cells (arrow). Scale bar = 20 μm. **G.** Adaxial leaf surface showing depressions indicating sinuous walled epidermal cells. Scale bar = 20 μm.

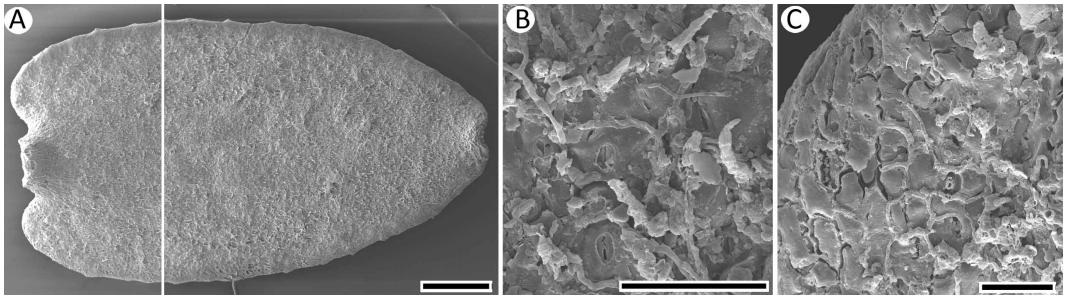

Fig. S18. Scanning electron micrographs of fossil leaves of *Epacriphyllum* species 9 (Ericaceae subfamily Styphelioideae) from Stony Creek Basin. Reproduced with permission from (3), with formatting slightly modified to make it consistent with other figures. **A.** Abaxial surface. Scale bar = 0.5 mm. This is a composite image (as indicated by white line). **B.** Abaxial surface showing stomata. Scale bar = 50 μm. The specimen shows some fungal overgrowth (the wavy hair-like structures). **C.** Partially eroded abaxial surface showing sinuous-walled epidermal cells. Scale bar = 50 μm.

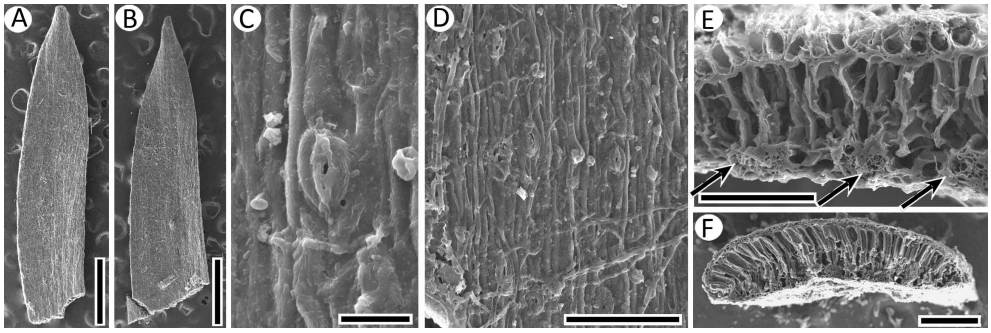

Fig. S19. Scanning electron micrographs of fossil leaves of *Epacriphyllum* species 10 (Ericaceae subfamily Styphelioideae) from Stony Creek Basin. Reproduced with permission from (3), with formatting slightly modified to make it consistent with other figures. **A, B.** Abaxial surface of leaves. Scale bar = 1 mm. **C.** Detail of abaxial surface showing a stoma. Scale bar = 20 μm. **D.** Detail of abaxial surface showing stomatal distribution. Scale bar = 100 μm. **E**. Cross section of leaf showing vascular bundles attached to the lower epidermis. Scale bar = 100 μm. **F.** Cross section of leaf. Scale bar = 200 μm.

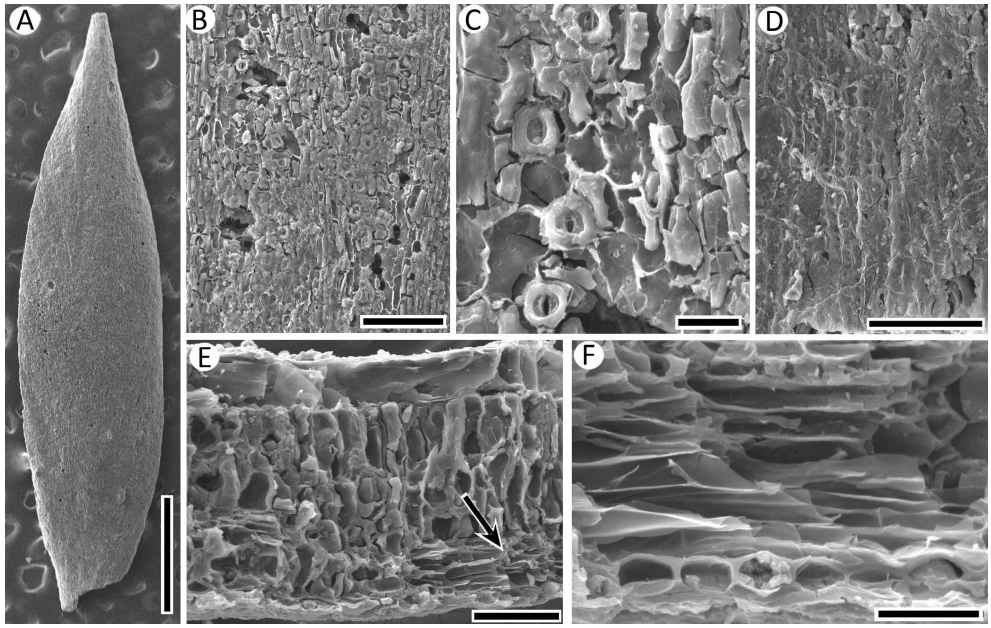

Fig. S20. Scanning electron micrographs of fossil leaves of *Epacriphyllum* species 11 (Ericaceae subfamily Styphelioideae) from Stony Creek Basin. Reproduced with permission from (3), with formatting slightly modified to make it consistent with other figures. **A.** Abaxial surface. Scale bar = 1 mm. **B.** Partially eroded abaxial surface showing stomatal distribution. Scale bar = 100 μm. **C.** Partially eroded abaxial surface showing stomata and weakly sinuous-walled epidermal cells. Scale bar = 20 μm. **D.** Adaxial surface showing sinuous-walled epidermal cells. Scale bar = 100 μm. **E.** Cross section showing tall adaxial epidermal cells. Note also vascular bundle adjacent to the abaxial epidermis (arrow). Scale bar = 50 μm. **F.** Cross section showing vascular bundle adjacent to the abaxial epidermis. Scale bar = 20 μm.

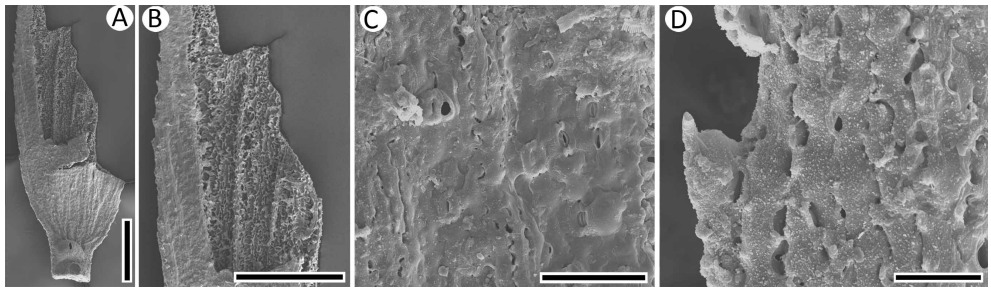

Fig. S21. Scanning electron micrographs of fossil leaves of *Epacriphyllum* species 12 (Ericaceae subfamily Styphelioideae) from Stony Creek Basin. Reproduced with permission from (3), with formatting slightly modified to make it consistent with other figures. **A**. Abaxial surface. Scale bar = 0.5 mm. **B.** Abaxial surface showing teeth, veins and stomatal distribution. Scale bar = 0.5 mm. **C.** Abaxial surface showing stomata and sinuous cell walls. Scale bar = 50 μm. **D.** Margin of abaxial surface showing a tooth/trichome base. Scale bar = 20 μm.

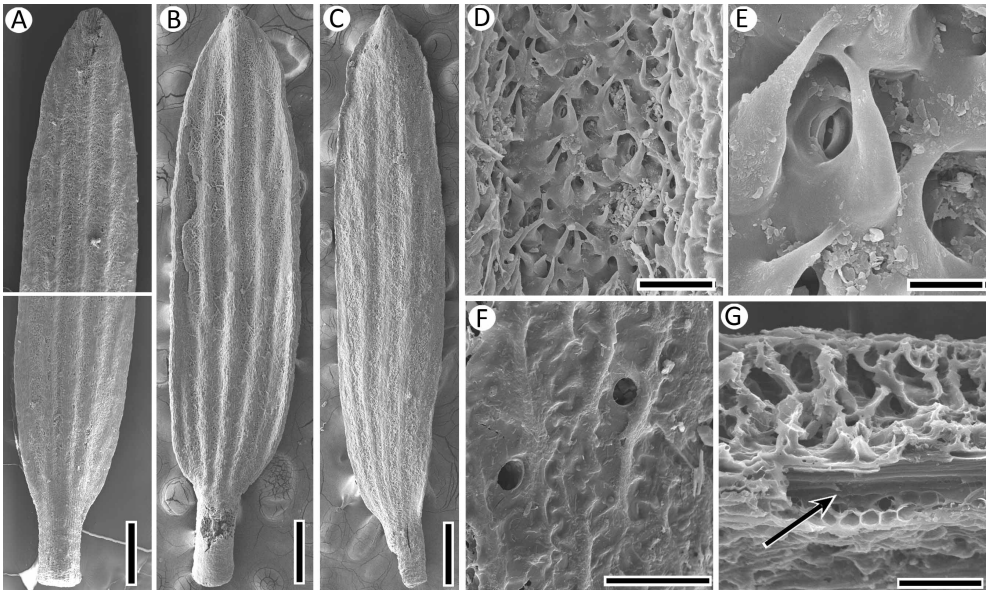

Fig. S22. Scanning electron micrographs of fossils of *Epacriphyllum* species 13 (Ericaceae subfamily Styphelioideae) from Stony Creek Basin. Reproduced with permission from (3), with formatting slightly modified to make it consistent with other figures. **A-C.** Abaxial surface of leaves. Scale bar = 0.5 mm. A is a composite image (as indicated by white line). **D**. Abaxial surface of a leaf showing stomata and trichomes restricted to interveinal regions, and sinuous epidermal cell walls of veinal regions. Scale bar = 50 µm. **E.** Abaxial surface of a leaf showing a stoma and trichomes. Scale bar = 10 µm. **F**. Adaxial surface of a leaf showing sinuous epidermal cell walls. Scale bar = 20 µm. **G.** Cross section of a leaf showing a vascular bundle adjacent to the abaxial epidermal cells. Scale bar = 50 µm.

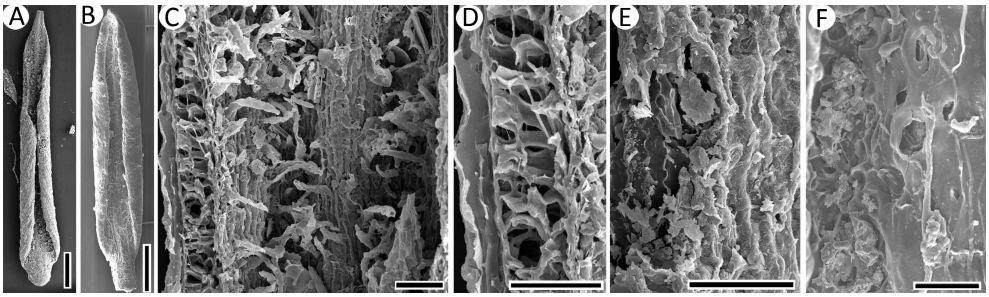

Fig. S23. Scanning electron micrographs of fossil leaves of *Epacriphyllum* species 14 (Ericaceae subfamily Styphelioideae) from Stony Creek Basin. Reproduced with permission from (3), with formatting slightly modified to make it consistent with other figures. **A.** Abaxial surface of leaf. Scale bar = 0.5 mm. **B.** Abaxial surface of leaf. Scale bar = 0.5 mm. **C.** Upper part of abaxial surface of leaf showing revolute margins and long trichomes. Scale bar = 50 µm. **D.** Longitudinal section of leaf showing the tall epidermal cells and tall mesophyll. Scale bar = 50 µm. **E.** Adaxial surface of leaf showing the elongate epidermal cells with sinuous walls. Scale bar = 50 µm. **F.** Upper part of abaxial surface of leaf showing stomata. Scale bar = 50 µm.

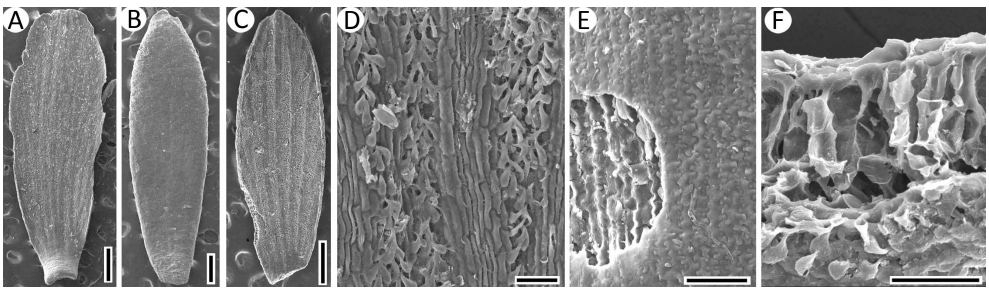

Fig. S24. Scanning electron micrographs of fossil leaves of *Epacriphyllum* species 15 (Ericaceae subfamily Styphelioideae) from Stony Creek Basin. Reproduced with permission from (3), with formatting slightly modified to make it consistent with other figures. **A-C**. Abaxial surface of leaves. Scale bar = 0.5 mm. **D.** Abaxial surface of leaf showing stomata and trichomes restricted to interveinal regions, and sinuous epidermal cell walls of veinal regions. Scale bar = 50 µm. **E.** Adaxial surface of leaf showing sinuous epidermal cell walls. Part of the surface has been eroded. Scale bar = 50 µm. **F.** Cross section of leaf showing epidermal and mesophyll cells. Scale bar = 50 µm.

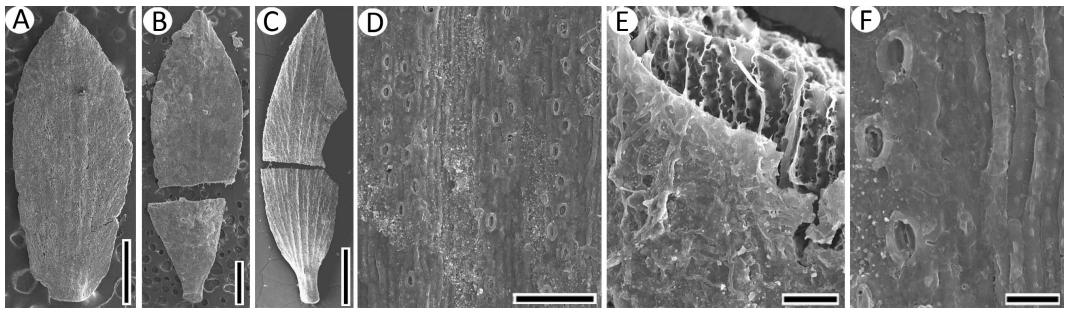

Fig. S25. Scanning electron micrographs of fossil leaves of *Epacriphyllum* species 16 (Ericaceae subfamily Styphelioideae) from Stony Creek Basin. Reproduced with permission from (3), with formatting slightly modified to make it consistent with other figures. **A-C**. Abaxial surface of leaves. Scale bar = 1 mm. **D.** Abaxial surface of leaf showing stomata restricted to interveinal regions, and sinuous epidermal cell walls of veinal regions. Scale bar = 100 μm. **E.** Partially eroded adaxial surface of leaf showing sinuous epidermal cell walls. Scale bar = 50 μm. **F.** Abaxial surface of leaf showing small papillae on interveinal region. Scale bar = 20 μm.

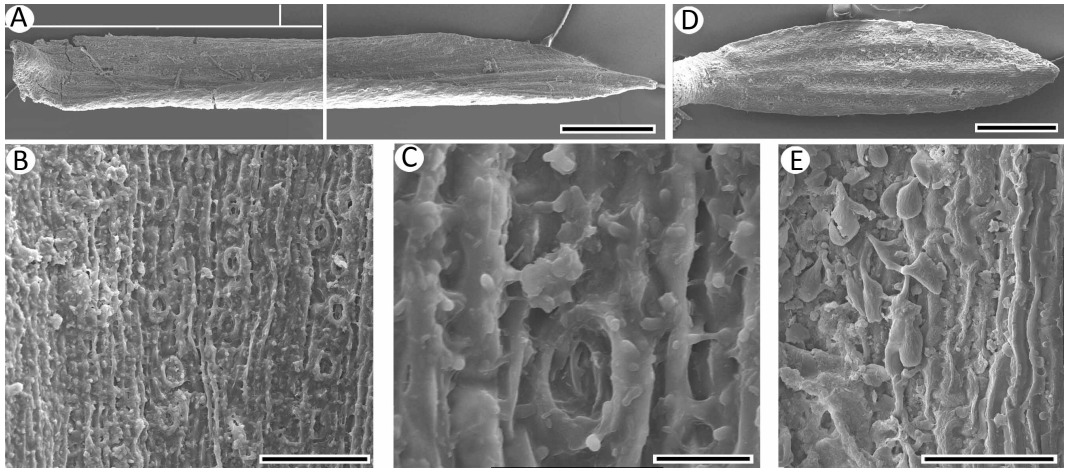

Fig. S26. Scanning electron micrographs of fossil leaves of *Epacriphyllum* species 17 and 18 (Ericaceae subfamily Styphelioideae) from Stony Creek Basin. Reproduced with permission from (3), with formatting slightly modified to make it consistent with other figures. **A.** Abaxial leaf surface of *Epacriphyllum* species 17. Scale bar = 0.5 mm. This is a composite image (as indicated by white lines). **B.** Abaxial leaf surface of *Epacriphyllum* species 17 showing aligned stomata restricted to interveinal regions, and sinuous epidermal cell walls of veinal regions. Scale bar = 50 μm. **C.** Abaxial leaf surface of *Epacriphyllum* species 17 showing a stoma and degraded waxes. Scale bar = 10 μm. **D.** Abaxial leaf surface of *Epacriphyllum* species 18. Scale bar = 0.5 mm. **E.** Abaxial leaf surface of *Epacriphyllum* species 18 showing outlines of sinuous-walled epidermal cells, stomata aligned parallel to the midrib and obscured by conical trichomes. Scale bar = 50 μm.

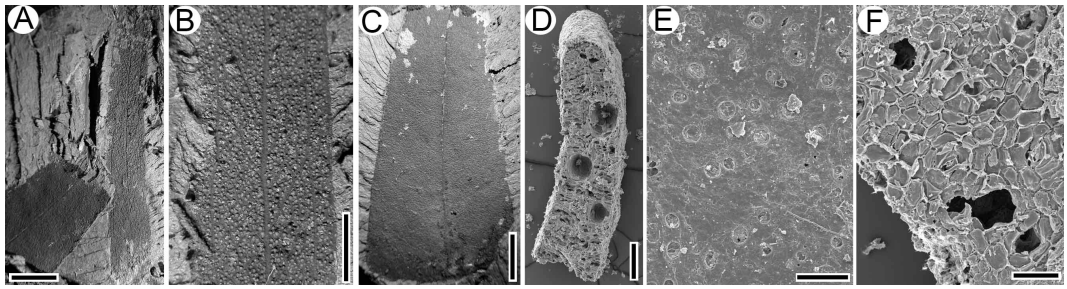

Fig. S27. Fossils consistent with *Eucalyptus* (Myrtaceae) from Stony Creek Basin. **A.** Leaves of species 1 and species 2 on the same plane. Scale bar = 10 mm**. B.** Leaf of species 1. Note the strong intramarginal veins, and secondary veins leading directly to the intramarginal vein. These are typical of *Eucalyptus*. Scale bar = 5 mm. **C.** Leaf of species 2. Scale bar = 10 mm. **D.** Scanning electron micrograph of a fragment of a leaf of species 2 in cross section, showing the isolateral leaves and prominent oil glands. Scale bar = 200 μm. **E.** Scanning electron micrograph of outer leaf surface species 2, showing the smooth surface and stomata. Scale bar = 200 μm. **F.** Scanning electron micrograph of inner surface of leaf cuticle of species 2, showing the stomatal complexes and epidermal cells. Scale bar = 50 μm.

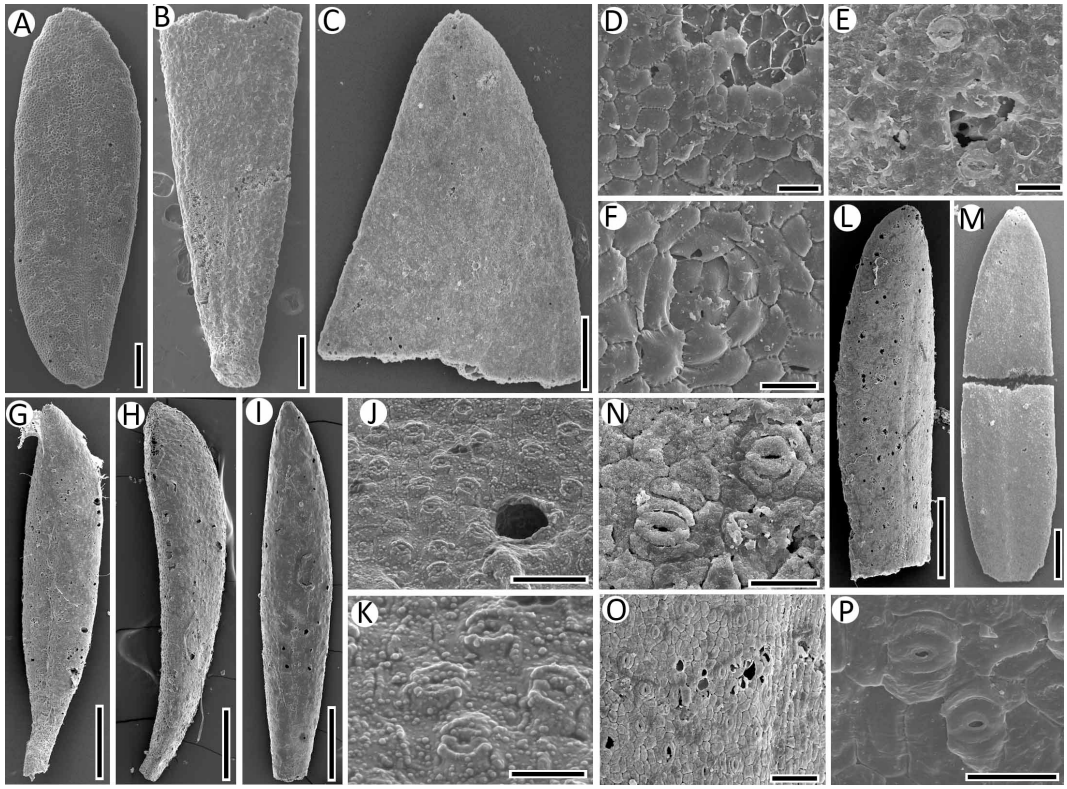

Fig. S28. Scanning electron micrographs of leaves consistent with Myrtaceae from Stony Creek Basin (I). **A-C.** Leaf fragments of Myrtaceae species 1. Scale bars = 0.5 mm. This species covers a wide range of leaf shapes, but the characteristic is that it is hypostomatic. Most sclerophyll Myrtaceae (and all other Myrtaceous species described here) are amphistomatic. **D.** Myrtaceae species 1. Adaxial surface showing the very distinctive epidermal cells. Scale bar = 50 µm. **E.** Myrtaceae species 1. Adaxial surface showing the distinctive lid cells covering an oil gland. Note also the buttresses connecting epidermal cells. Scale bar = 50 µm. **F.** Myrtaceae species 1. Abaxial surface showing stomata. Scale bar = 20 µm. **G-I.** Leaves of Myrtaceae species 2. Scale bars = 0.5 mm. This species differs from species 11 in having prominently ornamented cuticles (with papillae), whereas Myrtaceae species 11 has a smooth, waxy surface. **J.** Myrtaceae species 2. Abaxial surface showing stomata and epidermal cells. Scale bar = 50 µm. **K.** Abaxial surface showing stomata and epidermal cells. Note the papillae Scale bar = 20 µm. **L-M.** Leaves of Myrtaceae species 11. Scale bars = 0.5 mm. **N.** Myrtaceae species 11. Abaxial surface showing stomata and epidermal cells. Scale bar = 20 µm. **O.** Myrtaceae species 11. Abaxial surface showing stomata and epidermal cells. Scale bar = 50 µm. **P.** Myrtaceae species 11. Abaxial surface showing stomata and epidermal cells. Scale bar = 20 µm. This is interpreted as being a slightly eroded surface.

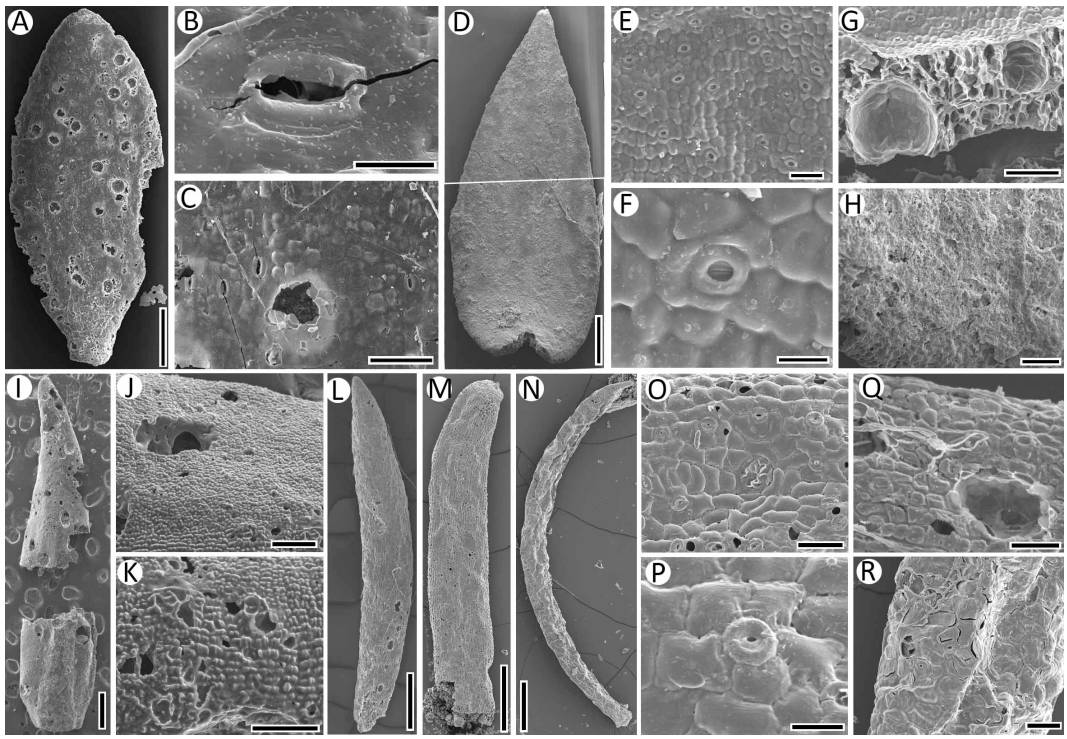

Fig. S29. Scanning electron micrographs of leaves consistent with Myrtaceae from Stony Creek Basin (II). **A.** Myrtaceae species 15, abaxial surface of leaf. Note the lack of a visible midrib. Scale bar = 0.5 mm. **B.** Detail of Myrtaceae species 15, showing a stoma. Scale bar = 20 µm. **C.** Detail of Myrtaceae species 15, showing stomata and epidermal cells. Scale bar = 100 µm. **D.** Myrtaceae species 3, adaxial surface of leaf. This is a composite image (as indicated by white line). Scale bar = 0.5 mm. This species resembles some species of *Leptospermum* and is distinctive in the combination of leaf shape and being hypostomatic. **E.** Detail of abaxial leaf surface of Myrtaceae species 3, showing stomata and epidermal cells. Scale bar = 50 µm. **F.** Detail of abaxial leaf surface of Myrtaceae species 3, showing stomata and epidermal cells. Scale bar = 20 µm. **G.** Cross section of Myrtaceae species 3, showing oil glands, mesophyll cells, stomata and epidermal cells. Scale bar = 50 µm. **H.** Detail of adaxial leaf surface of Myrtaceae species 3, showing the lack of stomata. Scale bar = 50 µm. **I.** Leaf of Myrtaceae species 4. Note the distinctive shape. Scale bar = 0.5 mm. **J.** Detail of abaxial leaf surface of species 4. Note the lack of stomata. The surface is densely papillose, but it is possible that this is an artefact in this relatively modified fossil. Scale bar = 100 µm. **K.** Detail of margin of abaxial leaf surface of species 4, showing some stomata. Scale bar = 100 µm. **L-N.** Leaves of Myrtaceae species 5. Note the distinctive terete leaf form. Such leaves are common in the Australian sclerophyll flora Scale bar = 0.5 mm. **O.** Detail of leaf surface of species 5, showing stomata, epidermal cells, and gland. Scale bar = 50 µm. **P.** Detail of leaf surface of species 5, showing a stoma. Note the cyclocytic subsidiary cell arrangement. Scale bar = 20 µm. **Q.** Detail of leaf surface of species 5, showing stomata, epidermal cells, and gland. Scale bar = 50 µm. **R.** Detail of leaf surface of species 5, showing epidermal cells. Scale bar = 50 µm.

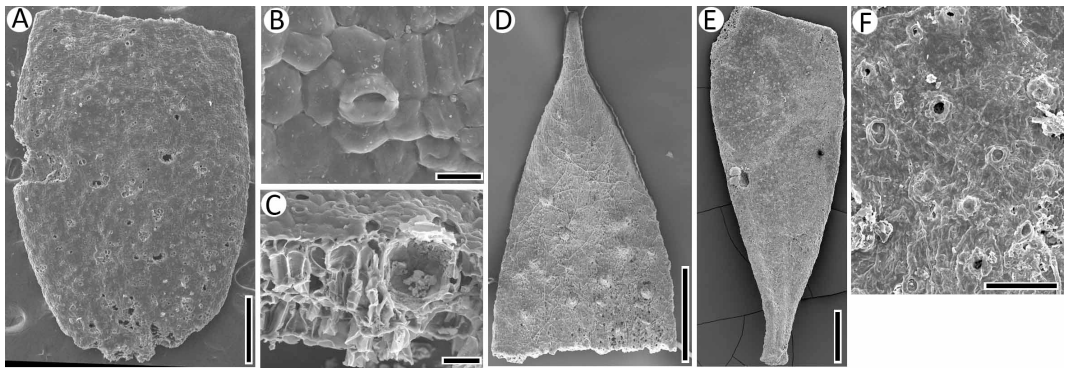

Fig. S30. Scanning electron micrographs of leaves consistent with Myrtaceae from Stony Creek Basin (III). **A.** Myrtaceae species 6, leaf base. Scale bar = 0.5 mm. This species differs from the other similar-sized Myrtaceous species described here in having cyclocytic stomata. **B.** Detail of Myrtaceae species 6, showing a stoma. Scale bar = 20 µm. **C.** Cross section of Myrtaceae species 6, showing oil gland and mesophyll tissue. Scale bar = 50 µm. **D.** Myrtaceae species 9 leaf apex. Scale bar = 0.5 mm. The presence of bulging oil glands and an acuminate leaf apex make this species distinctive. **E.** Myrtaceae species 13 leaf base. Scale bar = 0.5 mm. This acuminate leaf base is unlike any other species in this flora. **F.** Surface detail of Myrtaceae species 13, showing stomata. Scale bar = 50 µm.

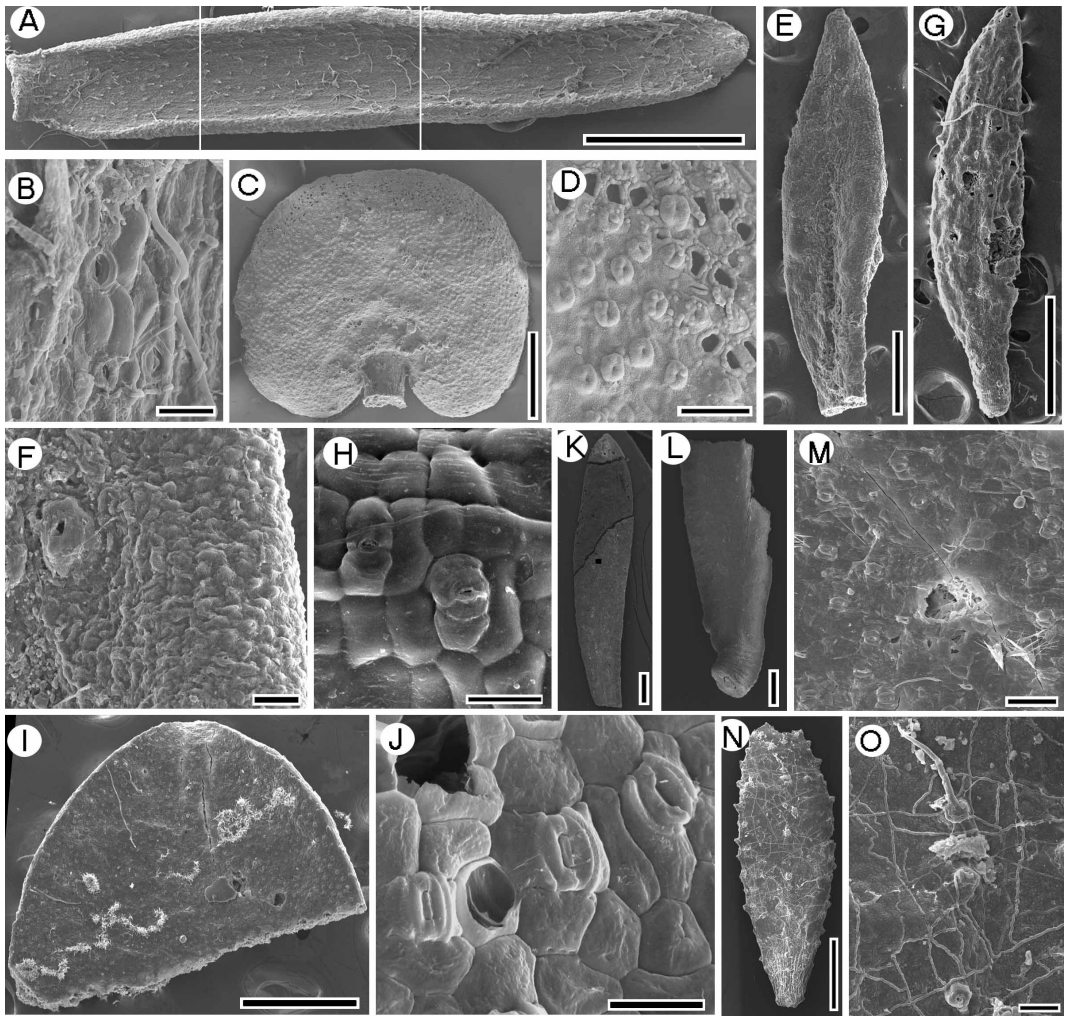

Fig. S31. Scanning electron micrographs of unattributed microphyllous leaves from Stony Creek Basin (I). **A**. Microphyll species 1, abaxial surface of leaf. Note the recurved margins and the lack of a visible midrib. This is a composite image (as indicated by white lines). Scale bar = 0.5 mm. **B.** Detail of microphyll species 1, showing stomata and epidermal cells. Scale bar = 20 µm. **C.** Microphyll species 3, abaxial surface of leaf. Note the orbicular shape and the lack of a visible midrib. Scale bar = 0.5 mm. **D.** Detail of microphyll species 3 showing stomata and epidermal cells. Scale bar = 50 µm. **E.** Microphyll species 4, adaxial surface of leaf. Note faintly visible midrib. Scale bar =0.5 mm. **F.** Detail from microphyll species 4, showing a stoma and the coarsely papillose surface. Scale bar = 50 µm. **G.** Leaf of microphyll species 5, abaxial surface of leaf. Note the lack of a visible midrib. Scale bar = 0.5 mm. **H.** Detail of microphyll species 5, showing stomata and epidermal cells. Scale bar = 20 µm. **I.** Microphyll species 7, abaxial surface of leaf. Scale bar = 0.5 mm. **J.** Detail of microphyll species 7, showing stomata and epidermal cells. Scale bar = 20 µm. **K.** Incomplete leaf of microphyll species 7A. Scale bar = 0.5 mm. This species differs from microphyll species 7, which has relatively similar stomatal morphology, in that the leaf apex is acute (as opposed to the very broad blunt apex of microphyll species 7), the leaf is narrower and the epidermis is striated. **L.** Leaf base of microphyll species 7A. Scale bar = 0.5 mm. **M.** Surface detail of microphyll species 7A showing stomata. Scale bar = 50 µm. **N.** Leaf of microphyll species 8. Scale bar = 0.5 mm **O.** Surface detail of microphyll species 8 showing distinctive trichomes and microscopically papillose surface. Scale bar = 20 µm.

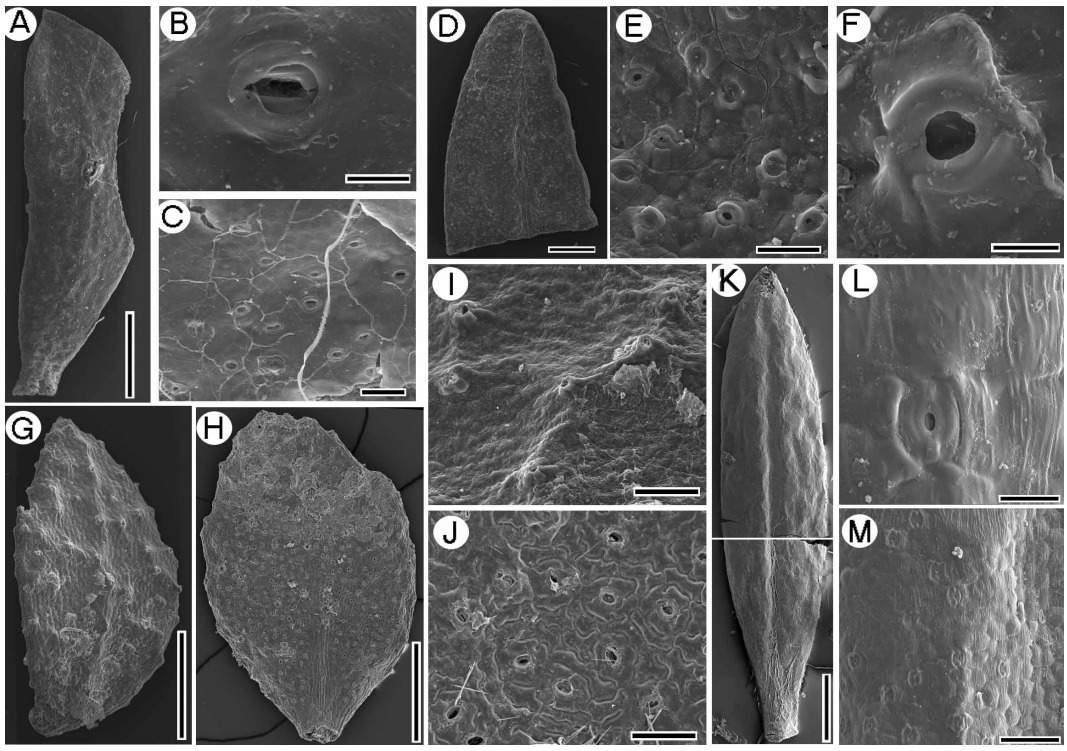

Fig. S32. Scanning electron micrographs of unattributed microphyllous leaves from Stony Creek Basin (II). **A.** Microphyll species 9, abaxial surface of leaf. Note the lack of visible midrib. Scale bar = 1.0 mm. The distinctive features of this microphyll species are the obovate, acute amphistomatic leaves, the relatively smooth epidermis and the stomata mostly aligned parallel to the major axis. Some of the Myrtaceae fossils are broadly similar, but have conspicuous oil glands, randomly aligned stomata and conspicuous epidermal papillae. **B.** Detail of microphyll species 9, showing a stoma and epidermal cells. Scale bar = 10 µm. **C.** Detail of microphyll species 9, showing stomata and epidermal cells. Scale bar = 50 µm. **D.** Microphyll species 11, abaxial surface of leaf. Note the visible midrib. Scale bar for = 0.5 mm. The distinctive features of this microphyll species are the raised stomata combined with the leaf size and shape. **E.** Detail of microphyll species 11, showing stomata and epidermal cells. Scale bar = 40 µm. **F.** Detail of microphyll species 11, showing a stoma. Scale bar = 10 µm. **G.** Microphyll species 12, adaxial surface of leaf. Note the visible midrib and raised glands. Scale bar = 0.5 mm. This is very distinctive - hypostomatic with conspicuous glands on the adaxial surface and unusual epidermal cell arrangement on the abaxial surface. **H.** Microphyll species 12, abaxial surface of leaf. Note the visible stomata. Scale bar = 0.5 mm. **I.** Detail of adaxial surface of microphyll species 12, showing glands and epidermal cells. Scale bar = 100 µm. **J.** Detail of abaxial surface of microphyll species 12, showing stomata and epidermal cells. Scale bar = 50 µm. **K.** Microphyll species 16, abaxial surface of leaf. Note the visible midrib. This is a composite image (as indicated by white line). Scale bar = 0.5 mm. **L.** Detail of microphyll species 16, showing a stoma. Note the striated epidermis Scale bar = 10 µm. **M.** Detail of microphyll species 16, showing stomata and epidermal cells. Note the stomata are aligned parallel to the midrib and the epidermal cells are polygonal. Scale bar = 50 µm.

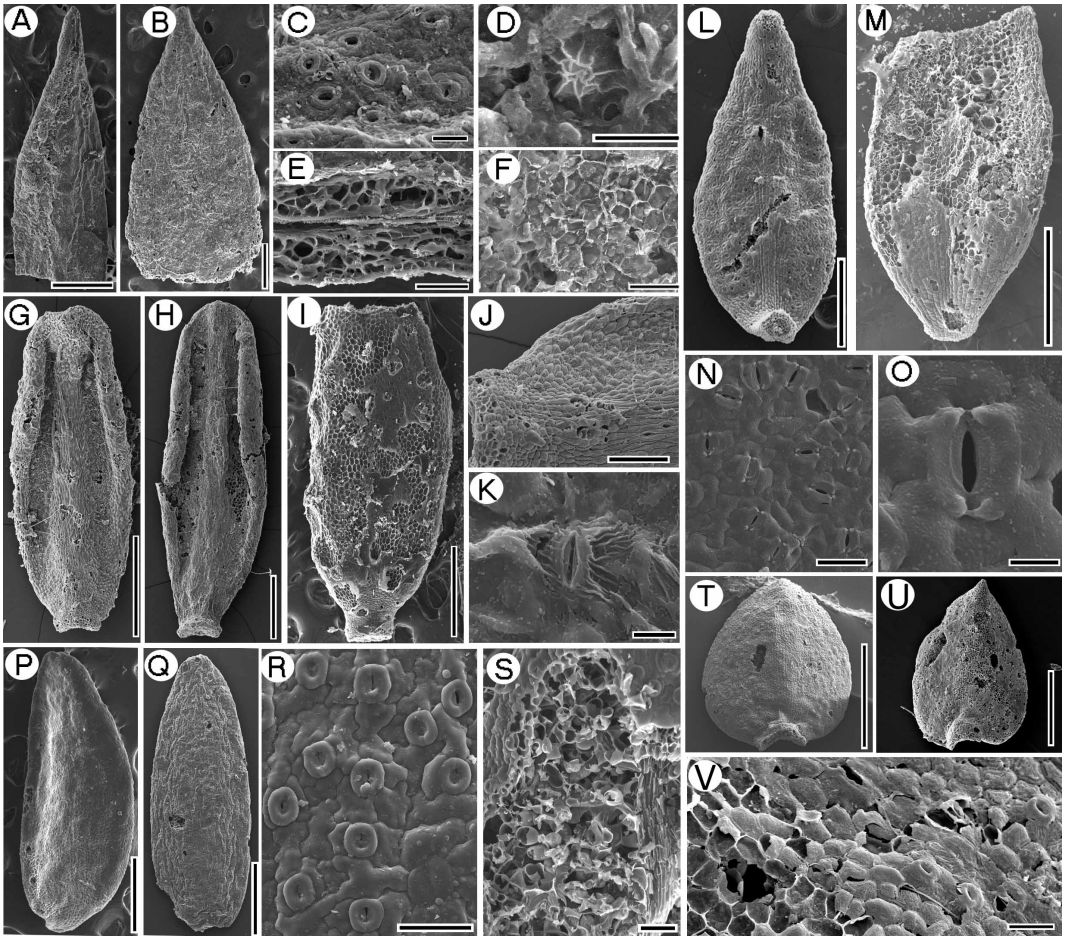

Fig. S33. Scanning electron micrographs of unattributed microphyllous leaves from Stony Creek Basin (III). **A.** Microphyll species 19, adaxial surface of leaf. Note the lack of a visible midrib. Scale bar = 0.5 mm. **B.** Microphyll species 19, abaxial surface of leaf. Scale bar = 0.5 mm. **C.** Detail of abaxial leaf surface of microphyll species 19, showing stomata. Scale bar = 50 µm. **D.** Detail of microphyll species 19, showing gland. Scale bar = 10 µm. **E.** Longitudinal section of microphyll species 19 showing mesophyll cells and spirally thickened vein cells. Scale bar = 50µm. **F.** Detail from adaxial leaf surface of microphyll species 19. Note the epidermal cells. Scale bar = 20 µm. **G-H.** Abaxial surface of leaves of microphyll species 25. Scale bar = 0.5 mm. **I.** Adaxial surface of a leaf of microphyll species 25. Scale bar = 0.5 mm. **J.** Detail of abaxial surface of a leaf of microphyll species 25 showing cells and stomata. Scale bar = 100 µm. **K.** Detail of abaxial surface of a leaf of microphyll species 25 showing a stoma. Scale bar = 10 µm. **L.** Abaxial surface of leaf of microphyll species 26. Scale bar = 0.5 mm. This species is clearly distinct from all other species in the samples - the stomata are of a unique form. **M.** Adaxial surface of leaf of microphyll species 26, showing the lack of stomata. Scale bar = 0.5 mm. **N.** Detail of abaxial surface of a leaf of microphyll species 26 showing cells and stomata. Scale bar = 50 µm. **O.** Detail of abaxial surface of a leaf of microphyll species 26 showing one stoma. Scale bar = 10 µm. **P.** Adaxial surface of a leaf of microphyll species 29. Scale bar = 0.5 mm. Unlike microphyll species 26, this species is amphistomatic. The stomata are also very different in form. **Q.** Abaxial surface of a leaf of microphyll species 29. Scale bar = 0.5 mm. **R.** Detail of abaxial surface of a leaf of microphyll species 29 showing cells and stomata. Scale bar = 50 µm. **S.** Fractured edge of a leaf of microphyll species 29 showing anatomy. Scale bar = 50 µm. **T-U.** Abaxial surfaces of leaves of microphyll species 32. Scale bars = 0.5 mm. **V.** Detail of abaxial surface of a leaf of microphyll species 32. Note the striate surface, raised stomata and straight walled epidermal cells. Scale bar = 50 µm.

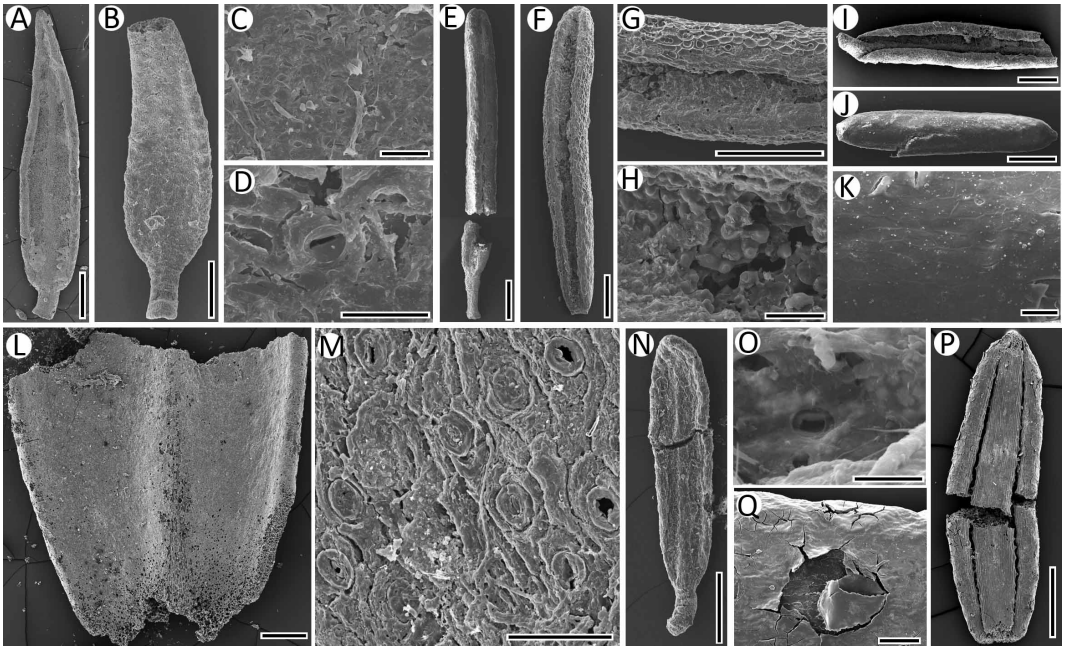

Fig. S34. Scanning electron micrographs of unattributed microphyllous leaves from Stony Creek Basin (IV). **A-B.** Microphyll species 31, two leaves. Note the incurved margins. Scale bar = 0.5 mm. **C.** Microphyll species 31, detail of abaxial surface of leaf showing stomata. Scale bar = 50 μm. **D.** Detail of leaf of microphyll species 31 showing a single stoma. Scale bar = 20 μm. **E.** Leaf of microphyll species 35. Note the thick, elongate leaf, almost square in cross section and with strongly revolute margins, and the well developed petiole. Scale bar = 0.5 mm. **F.** Leaf of microphyll species 36. Note the thick, elongate leaf with strongly revolute margins. This species differs from microphyll species 35 in being almost sessile and having an acute apex. The stomatal form suggests that this species may be a member of Fabaceae. Scale bar = 0.5 mm. **G.** Detail of leaf of microphyll species 36. Scale bar = 0.5 mm. **H.** Detail of leaf of microphyll species 36 showing stomata and papillose epidermal cells. Scale bar = 100 μm. **I.** Abaxial surface of a leaf of microphyll species 37. Scale bar = 0.5 mm. **J.** Adaxial surface of a leaf of microphyll species 37. Scale bar = 0.5 mm. **K.** Detail of adaxial surface of leaf of microphyll species 37, showing the polygonal epidermal cells, making this microphyll species distinct from some specimens of Ericaceae with similar leaf shape and also found at Stony Creek Basin. Scale bar = 50 μm. **L.** Adaxial surface of a leaf of microphyll species 42. Scale bar = 0.5 mm. **M.** Detail of abaxial surface of leaf of microphyll species 42, showing the highly distinctive stomata and epidermal cells. Scale bar = 50μm. **N.** Adaxial surface of a leaf of microphyll species 38. Scale bar = 0.5 mm. **O.** Detail of abaxial surface of leaf of microphyll species 38, showing one stoma. Scale bar = 10 μm. **P.** Adaxial surface of a leaf of microphyll species 40. Scale bar = 0.5 mm. **Q.** Detail of surface of leaf margin of microphyll species 40, showing area of exposed epidermal cells. Scale bar = 100 μm.

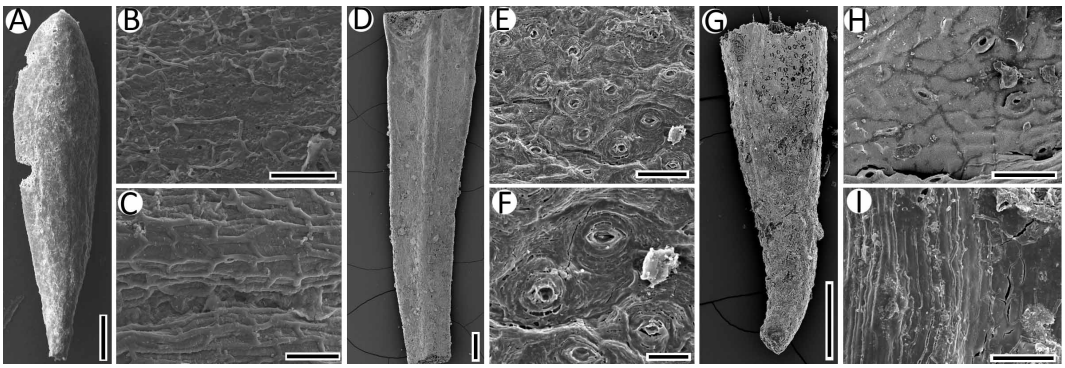

Fig. S35. Scanning electron micrographs of unattributed microphyllous leaves from Stony Creek Basin (V). **A.** Leaf of microphyll species 39. Scale bar = 0.5 mm. **B.** Microphyll species 39, detail of abaxial surface of leaf showing stomata and epidermal cells. Scale bar = 50 μm. **C.** Microphyll species 39, detail of adaxial surface of leaf showing elongate epidermal cells with prominent walls. Scale bar = 50 μm. **D.** Leaf base of microphyll species 43. Scale bar = 0.5 mm. **E.** Microphyll species 43, detail of surface of leaf showing stomata. Scale bar = 50 μm **F.** Microphyll species 43, detail of surface of leaf showing stomata. Scale bar = 20 μm **G.** Leaf base of microphyll species 44. Scale bar = 0.5 mm. **H.** Microphyll species 44, detail of surface of leaf showing stomata and epidermal cells. Scale bar = 50 μm **I.** Microphyll species 44, detail of surface of elongated epidermal cells. Scale bar = 50 μm

1. Wilson KL & Johnson LAS (1989) Casuarinaceae. *Flora of Australia*, ed George AS (Australian Government Publishing Service, Canberra), pp 100-203.
2. Jordan GJ (1997) Evidence of Pleistocene plant extinction and diversity from Regatta Point, western Tasmania, Australia. *Botanical Journal of the Linnean Society* 123:45-71.
3. Jordan GJ, Bromfield KE, Sniderman JMK, & Crayn D (2007) Diverse fossil epacrids (Styphelioideae; Ericaceae) from Early Pleistocene sediments at Stony Creek Basin, Victoria, Australia. *International Journal of Plant Sciences* 168:1359-1376.

Supporting Information

Sniderman et al. 10.1073/pnas.1216747110

SI Text

Environmental Information for Stony Creek Basin and Lake Dobson. Climatic estimates derived from ANUCLIM (1) for Stony Creek Basin (SCB) are mean annual temperature of *ca*. 11.0 °C and mean annual precipitation of *ca*. 880 mm. At SCB, regional vegetation today is primarily open forests and woodlands dominated by *Eucalyptus*. Species richness of these forests is relatively low by eastern Australian standards in terms of both woody and total plant species richness (2, 3). Regional soils constitute a mosaic of infertile soils developed on Paleozoic metasediments and moderately fertile soils developed on Plio-Pleistocene valley flow basalts. This mosaic largely controls patterns of vegetation productivity and floristics. Hence, basalt-derived soils originally supported forests with grassy understories but have largely been cleared for agriculture, and relatively infertile Paleozoic metasediments support native forest with variably grassy or woody understories. For Lake Dobson (LD), mean annual temperature is 6.2 °C, and mean annual precipitation is *ca*. 1,550 mm, with a slight bias to winter precipitation. At LD, the vegetation in the hydrological catchment is mainly subalpine *Eucalyptus* or conifer woodland, with an understory of evergreen angiosperm trees and shrubs dominated by members of the families Ericaceae, Proteaceae, and Asteraceae. Areas of subalpine–alpine sedgelands and heaths also occur in the catchment.

Fossil Sampling and Identification. The four samples (labeled according to field depths below a site datum, 170–200 cm), consisting of unlithified, black, silty clay laminated to massive sediments, were dispersed in a 6% (wt/vol) solution of $Na_4P_2O_7$ and gently wet-sieved over a 250-μm screen to retrieve plant macrofossils.

To make valid comparisons with the modern analog system used in this work (LD), our analyses of fossils were restricted to leaves. The fossil species were discriminated using gross morphology (size, shape, teeth, and veins) and microscopic features (Fig. 2 and *SI Appendix*, Figs. S3–S35). The observable features varied according to the preservation type—either full organic preservation or carbonization. Carbonized specimens often showed excellent surface detail and when eroded, epidermal cell structures. Furthermore, such leaves could be fractured to show highly detailed internal anatomy. Fossils with organic preservation showed excellent preservation of cuticle anatomy but little internal anatomy. Segregation of fossils into species was relatively conservative—where there was doubt, fossils were lumped into one species. For example, Fabaceae species 1 (*SI Appendix*, Fig. S6) includes leaves with both entire and crenate margins and smooth epidermal cells as well as epidermal cells topped by striated mounds. Similarly, Myrtaceae species 5 (*SI Appendix*, Fig. S31) is consistent with a wide range of morphologically convergent modern species. Several of the species of Ericaceae subfamily Styphelioideae include a wider range of leaf morphologies than might be expected from a random sample of leaves from a single population (4).

The fossils were analyzed with scanning EM using an FEI Quanta 600 ESEM (FEI) or a Hitachi SU-70 field emission scanning electron microscope (Hitachi). Whole specimens were mounted on aluminum stubs and then air-dried, sputter-coated with gold or platinum to a nominal thickness of 20 nm, and observed under high vacuum at 2.5–20 kV. Where possible, cuticles of organically preserved specimens were prepared by demounting part or all of the specimen, immersing in a 10% aqueous solution of Cr_2O_3 until only the cuticle remained, and rinsing. Cuticles were remounted on aluminum stubs, ensuring that all possible surfaces (for example, inner and outer surfaces of the adaxial and abaxial surfaces) were exposed, recoated, and then observed under scanning EM.

Estimation of the Asymptotic Species Richness of the Fossil Flora. We expected the observed diversity of the SCB fossil flora to underestimate the true fossil richness of the sedimentary strata from which it was recovered, particularly because the flora includes many rare species (23 species are known from only one specimen). Sampling theory suggests that a sample containing many rare species is likely to be an incomplete census of the richness of the source (5, 6). Several nonparametric techniques use the observed abundances of species in samples to estimate the asymptotic true richness of incompletely sampled biotas. Like rarefaction approaches (7), these techniques allow comparison between different floras by correcting for unequal sampling effort. However, the estimates of asymptotic richness avoid several problems inherent in rarefaction, including the need to make an arbitrary choice of sample size. We estimated the asymptotic richness of the SCB fossil flora using the abundance-based coverage estimator (ACE) (8, 9), because ACE is recommended as a point estimate of species richness for heterogeneous assemblages, such as the SCB assemblages, in which species have highly unequal detection probabilities (8–10).

To quantify the extent to which the observed fossil flora is an incomplete sample of the true species richness of the fossil flora, we calculated the additional sampling effort necessary to reach $\hat{S}$, the asymptote of the species accumulation curve, using a sampling effort estimator from ref. 11 (Table S1). This inferential method estimates the number of additional individuals m that would have to be observed for the number of singletons to drop to zero. For singleton-rich assemblages, this number is likely to be large, because it can be expected that new singletons will be observed before all singletons in the original sample have been observed at least two times (6, 11). We, therefore, also estimated the additional sample size required to reach mg, a user-determined fraction of $\hat{S}$, where $0 < g < 1$ and $g > S/\hat{S}$ (11). The additional sampling effort to reach asymptotic species richness for SCB is estimated as 13,749 additional specimens; to reach 95% of asymptotic richness ($g = 0.95$), 4,401 additional specimens would be required. These estimates should be viewed with caution, because the sampling effort estimator uses only the Chao1 nonparametric abundance estimator (5), which we did not use for estimating fossil richness, because both the ACE estimator is more appropriate for heterogeneous samples and the ACE estimate (90.5 species) is here considerably more conservative than the Chao1 estimate (123 species). However, the result confirms that the observed fossil flora represents a substantially incomplete census of the body of sediment from which it was recovered.

Relationship Between Fossil and Source Flora. We analyzed the relationship between extant sclerophyll vegetation in the hydrological catchment of LD and recently deposited leaf assemblages recovered from surface sediments within the lake. We reidentified all specimens from the samples of Hill and Gibson (12) as a basis for diversity calculations (Table S2). We surveyed the floristics of the vegetation surrounding LD and found 58 species of woody, sclerophyllous dicots in the catchment.

To make an equal sampling effort comparison of the richness of the SCB fossil flora and the LD leaf assemblage, we estimated the asymptotic richness of the LD leaf assemblages using nonparametric asymptotic species-richness estimators. We also compared richness using rarefaction curves and the Michaelis–Menten functional extrapolation (6) (Table S2). We separately analyzed

the entire LD dataset and subsets of the data from the lake margin (zone L-2 of Fig. S2) and deeper water in the center of LD (zone L-1 of Fig. S2), which represent spatially and floristically distinct sets of samples separated by an interval of lower leaf richness. However, the results in the text refer only to the lake center subset (central LD), because this part of the lake represents the closest sedimentological analog for the four SCB samples, which were deposited in a quiet sedimentary environment in deep water near the center of paleolake SCB (13). The LD samples, with low observed (for central LD, $S = 17$) and estimated ($\hat{S}$ ACE = 18.2) species richness, are clearly less species-rich than the SCB fossil flora, regardless of which asymptotic estimate is used or whether comparisons are made using rarefaction or its functional extrapolation. This result is confirmed by rarefaction curves for LD (Fig. S1), which imply that few species remain undiscovered in this well-documented assemblage (for central LD, $n = 6{,}153$).

Woody species richness of the LD catchment is 58 species, and ACE asymptotic species richness of the central LD samples is 18.2 [95% confidence interval (CI) = 17.1–27.0] species. Hence, the proportion of the source flora represented in the central LD leaf assemblage is 18.2/58 = 0.314 (95% CI = 0.29–0.47). Assuming that a similar proportion of the Early Pleistocene source flora is represented in the SCB fossil flora, the woody species richness of the SCB source vegetation was

$$\frac{\hat{S}_{SCB}}{\hat{S}_{LD}} \times S_{LDveg} = S_{SCBveg} \text{ or } \frac{90.5}{18.2} \times 58 = 288 \text{ species},$$

where $\hat{S}_{SCB}$ and $\hat{S}_{LD}$ are ACE asymptotic estimates of the species richness of the SCB fossil flora and central LD leaf assemblages, respectively, and S_{LDveg} and S_{SCBveg} are woody species richness within the hydrological catchments of LD today and SCB during the Early Pleistocene, respectively.

CIs associated with asymptotic richness estimates (8) are asymmetrical to ensure that the lower confidence limit CL_L remains greater than S. Chao (14) developed 95% CIs for asymptotic estimators based on log transformation of $\hat{S}$–S and the SE of $\hat{S}$. Hence, using equation 12 in the work by Chao (14), a log-normal CI for an ACE estimate is

$$\left[S + (\hat{S} - S)/C, S + (\hat{S} - S) \times C\right],$$

where

$$C = \exp\left\{ z \left[\log\left(1 + \frac{\sigma^2}{(\hat{S} - S)^2} \right) \right]^{0.5} \right\}$$

and z is a normal distribution z score corresponding to the desired $(1 - \alpha)$ CI. To estimate a 95% CI for the ratio $\hat{S}_{SCB}/\hat{S}_{LD}$, we used a 1 million member Monte Carlo simulation of the ratio, assuming log normality and full independence between SCB and LD. This simulation provided us with a 95% CI of 3.09–6.56. We assume that our estimate of $S_{LDveg} = 58$ has zero error; thus, a 95% CI for S_{SCBveg} is

$$[CL_L \times 58, \;\; CL_U \times 58] = [179, 380].$$

To increase confidence in our species richness estimate of SCB Early Pleistocene source vegetation, we estimated this richness in three other ways. First, although we consider the central LD samples the best analog for the SCB fossil samples, we calculated the asymptotic richness of the lake margin LD samples and all of the LD samples and used these results as the basis for separate estimates of the SCB source vegetation richness. These results (marginal LD $\hat{S} = 20.7$ species; all LD samples $\hat{S} = 21.6$) (Table S2) result in slightly lower estimates of SCB source richness of 254 (95% CI = 193–332) and 243 (95% CI = 120–322) species, respectively. Second, we used rarefaction as an alternative way to compare the richness of the SCB fossil flora and the central LD leaf assemblages on the basis of constant sampling effort. Rarefied to the sampling effort of the SCB fossil flora ($n = 1{,}118$), the species richness of the central LD leaf assemblages is 13.02 species. This result implies that the richness of SCB source vegetation was

$$\frac{69}{13.02} \times 58 = 308 \text{ species}.$$

A somewhat lower estimate of 240 species is derived if the estimate is based on all LD samples (richness of all LD samples rarefied to 1,118 species =16.7 species) (Table S2). We also used the Michaelis–Menten functional extrapolation of rarefaction of SCB and central LD floras (Table S2) to estimate the richness of the SCB source vegetation as

$$\frac{106.8}{17.53} \times 58 = 353 \text{ species}.$$

Third, although the vegetation around LD represents the most plausible known physiognomic analog for the SCB fossil flora, it is uncertain whether the proportion of the SCB source vegetation represented in the SCB fossil flora was actually as low (0.314) as indicated by the central LD samples. Several studies have examined relationships between the diversity of leaf assemblages recovered from surficial lake sediments and their source floras (15–19). However, we were able to calculate asymptotic leaf richness and therefore, make comparisons on the basis of equal sampling effort for only one published study from a relatively small lake in New Zealand, Lady Lake (16). We made separate asymptotic richness estimates for leaf assemblages from individual sampling transects of Lady Lake (Table S2). Based on these transects, the proportion of source floras represented by the Lady Lake leaf assemblages ranges from 0.260 to 0.473 (mean = 0.377). With a mean asymptotic richness estimate for the three transects of 19.6 species and source vegetation richness for Lady Lake of 52 species, we can estimate SCB source richness using the SCB ACE estimate as

$$\frac{90.5}{19.6} \times 52 = 240 \text{ species} (95\% \text{ CI } 168 - 327).$$

Comparison with Extant Sclerophyll Biomes. Published detailed floristic data at the spatial scale of the SCB source catchment (10–100 ha) are rare to nonexistent in the southern hemisphere, even for the most completely studied and richest sclerophyll vegetation. In Australia, we, therefore, compiled floristic survey data for areas of known high sclerophyll species richness in Victoria (Grampians National Park, Anglesea Heath), New South Wales (Blue Mountains World Heritage Area), and the Southwest Floristic Region (SWFR) using vegetation databases associated with each region (20, 21) (NatureMap, http://naturemap.dec.wa.gov.au/default.aspx). For the Cape Floristic Region (CFR), we extracted woody species richness data from published checklists (22–28).

At large spatial scales, we analyzed the floras of especially rich national parks and Interim Biogeographic Regionalisation of Australia subregions (http://www.environment.gov.au/parks/nrs/science/bioregion-framework/ibra/index.html). At smaller scales, we identified areas with relatively high concentrations of survey localities, many of which represent standard quadrant surveys. Within these areas, we used Geographic Information System (GIS) techniques to extract species lists within measured polygons of a range of sizes. Wherever floristic sampling density was sufficient over a range of spatial scales, we defined hierarchically nested polygons, be-

cause species–area curves should ideally be constructed from survey of contiguous areas (29). However, existing floristic survey data are typically patchily distributed and characterized by collecting biases such as spatial clustering of surveys (for example, along roads or accessible topography). Hence, in data mining such databases at 1- to 100-ha scales, it was necessary to adopt an opportunistic rather than systematic approach. We searched for and excluded processing or geocoding artifacts; one such artifact is the attribution of large numbers (typically hundreds) of species to a single geocoded point, which probably arises through the databasing of old records labeled with only a generalized locality (for example, "Mt. Stirling"). To avoid as many of these errors as possible, we excluded most pre-1970 records. For comparison with the SCB woody fossil flora, we scored all dicotyledonous species by woody, herbaceous, or succulent habit based on our own knowledge and guided by information in regional floras (22, 30–32), FloraBase, the Western Australian Flora (http://florabase.dec.wa.gov.au/), and the New South Wales Flora Online (http://plantnet.rbgsyd.nsw.gov.au/floraonline.htm). Omission of monocotyledonous and herbaceous and succulent dicotyledonous taxa excludes an ecologically important component of the floras of species-rich sclerophyll vegetation. However, sclerophyll shrublands are characterized by high proportions of perennial evergreen woody dicots (33–35).

We calculated ordinary least squares linear regressions describing $\log_{10}$ species/area curves for southeast Australia, SWFR, and CFR (Fig. 3). We visually pruned these datasets to include only the richest sites for each region, because we were not interested in the average sclerophyll richness of regions but only those surveys and collections of surveys that captured the highest richness with respect to area. This pruning step was necessary, because when extracting data from online databases, many polygons may have had relatively low richness simply because of inadequate collections. Our species/area curves, thus, represent models of the highest known richness of woody sclerophyll vegetation within these three regions across several orders of magnitude in area.

CFR and SWFR had much higher extant woody plant species richness than eastern Australia. The least squares regression slopes for SWFR ($F = 19.89$, $P < 0.0001$) and CFR ($F = 10.78$, $P = 0.0014$) were significantly steeper than for eastern Australia (Fig. 3), indicating that species accumulate more rapidly in both SWFR and CFR than eastern Australia, as progressively larger regions are sampled (36). This result was expected, because both SWFR and CFR are considered to have higher sclerophyll species richness than eastern Australia at both local and regional scales (37, 38). That is, β-diversity is much higher in SWFR and CFR than the richest eastern Australian sclerophyll vegetation. This result confirms previous claims that the extraordinary richness of SWFR is largely a product of unusually high β-diversity (33), which has also been noted in comparisons of the western vs. eastern CFR (34, 36). The similar woody plant richness observed in CFR and SWFR was unexpected, because CFR has higher total plant species richness [≥9,030 species (22)] than SWFR [>7,380 species (33)]. However, comparisons of the regional lists suggest that the overall differences are driven by much richer succulent and herbaceous components in CFR [~55% of the total flora (22)] than SWFR (~37%; data from the Department of Environment and Conservation: http://florabase.dec.wa.gov.au).

Assessment of Time Averaging. Our four samples of fossils from SCB collectively represent *ca*. 2,500 y of ecological history, with individual samples each representing *ca*. 635 y (39). This duration is greater than most woody plant generation times, and we realized that our samples could incorporate temporal changes in local community composition resulting from either environmental change or repeated stochastic sampling of the regional species pool by the local source vegetation. Tomasovych and Kidwell (40) suggested that, because fossil assemblages typically have lower temporal resolution than samples of living communities, time-for-space substitution implies that fossil assemblages will also typically have lower spatial resolution than living assemblages. Hence, some of the between-habitat variability in the living community (β-diversity) may have been incorporated into a single fossil sample, where it will be interpreted as within-habitat α-diversity, thus effectively transferring diversity from β- to α-levels (40). If so, observed α-diversity may be unrealistically high relative to true ecologically instantaneous diversity.

We tested whether temporal resolution was a probable source of bias at SCB first by examining the relationship between sample stratigraphic thickness and α-diversity. We combined the floras of adjacent samples into progressively thicker pooled samples. If time averaging has masked β-diversity and increased apparent α-diversity, observed α-diversity of samples should increase and observed β-diversity should decrease with increasing sample thickness. However, the relationship was insignificant (Shannon α-diversity vs. sample stratigraphic thickness, $r = 0.150$, $P = 0.679$), providing no reason to believe that α-diversity would be lower if potential sample time averaging (sample thickness) was reduced beyond the 10 cm of our current samples. We also assessed whether there was any evidence for secular ecological change within the 170- to 200-cm sequence, which depending on its nature and direction, might either compound or mask any stochastic changes in species composition. We, thus, examined the relationship between intersample stratigraphic distance and either intersample similarity or intersample β-diversity. The relationships were insignificant (Table S4).

We analyzed the SCB fossil flora by partitioning its diversity into components analogous to α-, β-, and γ-diversity. Our partitioning approach substitutes time for space in an analogy with biodiversity partitioning methods used to analyze species diversity at plots to regional spatial scales (41–43). Our use of this spatial framework is consistent with evidence that the processes of species accumulation in space and time are fundamentally equivalent (44) and paleontological use of the framework to investigate diversity changes over time (45, 46). We calculated the Shannon diversity of each sample and the pooled fossil flora (Table S5). We interpreted the Shannon diversity of each sample as a measure of ecological-scale α-diversity (in analogy with individual floristic surveys), and we interpreted their pooled diversity as a measure of γ-diversity (in analogy with multiple surveys of a region). As shown by Jost (41), Shannon diversity H,

$$H = -\sum_{i=1}^{S} p_i \log p_i,$$

is a standard diversity index H of order one. However, when sampling is incomplete in communities containing many rare species, both species richness (true diversity of order zero) and Shannon diversity (true diversity of order one) suffer from negative biases or strongly underestimate diversity (47, 48). We, therefore, calculated Shannon diversities using a correction $\hat{H}$ suggested by Chao and Shen (47) (Table S5) based on unequal probability sampling theory, which compensates for loss of information based on the relative abundance of rare species:

$$\hat{H} = -\sum_{i=1}^{n} \frac{\hat{C}p_i \log\left(\hat{C}p_i\right)}{1-\left(1-\hat{C}p_i\right)^n},$$

where $\hat{C}$ is an estimate of sample coverage, the fraction of total abundances of discovered species, estimated as

$$\hat{C} = 1 - \left(\frac{f_1}{n}\right),$$

where f_1 is the number of singletons. We estimated the α-diversity of the four SCB samples as their mean α-diversity $\hat{H}_\alpha$ and the

γ-diversity of the samples as $\hat{H}_\gamma$. Following Jost (41), β-diversity is the difference between these measures:

$$\hat{H}_\beta = \hat{H}_\gamma - \hat{H}_\alpha.$$

However, to provide ecologically meaningful estimates of β-diversity, Jost (41) showed that Shannon β-diversity must be converted into its numbers equivalent $D(H_\beta) = \exp(H_\beta)$, which has the important property that it can effectively be interpreted in terms of the number of distinct communities present. Hence, for n more or less equal-sized communities, which have no shared species, $D(H_\beta) \approx n$, and for n identical communities, $D(H_\beta) \approx 1$.

To provide a baseline of β-diversity that could be expected simply from random sampling of the pooled flora, we evaluated the significance of observed β-diversity $\hat{H}_\beta$ by estimating the magnitude of $\hat{H}_\beta$ from random samples of the fossil flora using a resampling approach. We used a randomization test (49) to test whether our estimated $D(\hat{H}_\beta)$ differed significantly from one (i.e., zero β-diversity). We randomized the fossil observations 1,000 times, constraining them to have four populations of the same size as the four real samples from SCB. We then calculated $D(\hat{H}_\beta)$ from each replicate. We determined the probability that observed $D(\hat{H}_\beta)$ could arise simply from random sampling as the number of times that the randomized estimate exceeded our estimate of $D(\hat{H}_\beta)$ divided by 1,000.

Calculated $\hat{H}_\beta$ for the SCB fossil flora is 0.0254 or its numbers equivalent, $D(\hat{H}_\beta)$, 1.03. This result implies that there are effectively 1.03 distinct communities represented in the fossil flora, which implies that little time averaging has occurred. The randomization test estimated $P = 0.312$ for the null hypothesis that $D(\hat{H}_\beta) = 1$, and therefore, $D(\hat{H}_\beta)$ for the SCB fossil flora does not show significant β-diversity. Similar results were found from the randomization test of ordinary Shannon H_β, with observed $D(H_\beta) = 1.192$ and $P = 0.097$. Thus, differences between the SCB samples do not exceed that expected from random sampling of the pooled flora, and time averaging has not introduced a significant bias into the observed species richness of the fossil flora.

1. Xu T, Hutchinson M (2011) *ANUCLIM Version 6.1* (ANU Fenner School of Environment and Society, Canberra, Australia).
2. Rice B, Westoby M (1983) Plant species richness at the 0.1 hectare scale in Australian vegetation compared to other continents. *Vegetatio* 52(3):129–140.
3. Specht RL, Specht A (1989) Species richness of sclerophyll (heathy) plant communities in Australia—the influence of overstory cover. *Aust J Bot* 37(4):337–350.
4. Jordan GJ, Bromfield KE, Sniderman JMK, Crayn D (2007) Diverse fossil epacrids (Styphelioideae; Ericaceae) from Early Pleistocene sediments at Stony Creek Basin, Victoria, Australia. *Int J Plant Sci* 168(9):1359–1376.
5. Chao A (1984) Nonparametric estimation of the number of classes in a population. *Scand J Stat* 11(4):265–270.
6. Colwell RK, Coddington JA (1994) Estimating terrestrial biodiversity through extrapolation. *Philos Trans R Soc Lond B Biol Sci* 345(1311):101–118.
7. Gotelli NJ, Colwell RK (2001) Quantifying biodiversity: Procedures and pitfalls in the measurement and comparison of species richness. *Ecol Lett* 4(4):379–391.
8. Chao A, Lee S-M (1992) Estimating the number of classes via sample coverage. *J Am Stat Assoc* 87(417):210–217.
9. Chao A, Shen T-J (2010) *Program SPADE (Species Prediction and Diversity Estimation) Program and User's Guide*. Available at http://chao.stat.nthu.edu.tw. Accessed July 10, 2011.
10. Chazdon RL, Colwell RK, Denslow JS, Guariguata MR (1998) Statistical methods for estimating species richness of woody regeneration in primary and secondary rain forests of NE Costa Rica. *Forest Biodiversity Research, Monitoring and Modeling: Conceptual Background and Old World Case Studies*, eds Dallmeier F, Comiskey JA (Parthenon Publishing, Paris), pp 285–309.
11. Chao A, Colwell RK, Lin C-W, Gotelli NJ (2009) Sufficient sampling for asymptotic minimum species richness estimators. *Ecology* 90(4):1125–1133.
12. Hill RS, Gibson N (1986) Distribution of potential macrofossils in Lake Dobson, Tasmania. *J Ecol* 74(2):373–384.
13. Sniderman JMK (2011) Early Pleistocene vegetation change in upland south-eastern Australia. *J Biogeogr* 38(8):1456–1470.
14. Chao A (1987) Estimating the population size for capture-recapture data with unequal catchability. *Biometrics* 43(4):783–791.
15. McQueen DR (1969) Macroscopic plant remains in recent lake sediments. *Tuatara* 17 (1):13–19.
16. Drake H, Burrows C (1980) The influx of potential macrofossils into Lady Lake, north Westland, New Zealand. *N Z J Bot* 18(2):257–274.
17. Dunwiddie PW (1987) Macrofossil and pollen representation of coniferous trees in moden sediments from Washington. *Ecology* 68(1):1–11.
18. Spicer RA, Wolfe JA (1987) Plant taphonomy of late Holocene deposits in Trinity (Clair Engle) Lake, northern California. *Paleobiology* 13(2):227–245.
19. Allen JRM, Huntley B (1999) Estimating past floristic diversity in montane regions from macrofossil assemblages. *J Biogeogr* 26(1):55–73.
20. Viridans (2009) *Victorian Flora Information System* (Viridans Biological Databases, Melbourne).
21. Bedward M, Ellis M, Glesson P (2010) *Yet Another Vegetation Survey Database (YETI) Version 3.2* (NSW Department of Environment, Climate Change & Water). Available at www.environment.nsw.gov.au/research/Vegetationinformationsystem.html. Accessed November 15, 2011.
22. Goldblatt P, Manning JC (2000) Cape plants: A conspectus of the Cape flora of South Africa. Pretoria, South Africa: National Botanical Institute 9:1–744.
23. McDonald DJ, Morley M (1988) A checklist of the flowering plants and ferns of Swartboschkloof, Jonkershoek, Cape Province. *Bothalia* 18(2):261–270.
24. McDonald DJ (1999) The montane flora of the southern Langeberg, South Africa: A checklist of the flowering plants and ferns. *Bothalia* 29(1):119–137.
25. Kraaij T (2011) The flora of the Bontebok National Park in regional perspective. *S Afr J Bot* 77(2):455–473.
26. Cowling RM (1983) Diversity relations in Cape shrublands and other vegetation in the southeastern Cape, South Africa. *Vegetatio* 54(2):103–127.
27. Cowling RM (1990) Diversity components in a species-rich area of the Cape Floristic Region. *J Veg Sci* 1(5):699–710.
28. Cowling RM, Holmes PM, Rebelo AM (1992) Plant diversity and endemism. *The Ecology of Fynbos: Nutrients, Fire and Diversity*, ed Cowling RM (Oxford Univ Press, Oxford), pp 62–112.
29. Rosenzweig ML (1995) *Species Diversity in Space and Time* (Cambridge Univ Press, Cambridge, United Kingdom).
30. Walsh NG, Entwisle TJ (1994) *Flora of Victoria* (Inkata, Melbourne), Vol 2.
31. Walsh NG, Entwisle TJ (1996) *Flora of Victoria* (Inkata, Melbourne), Vol 3.
32. Walsh NG, Entwisle TJ (1999) *Flora of Victoria* (Inkata, Melbourne), Vol 4.
33. Hopper SD, Gioia P (2004) The southwest Australian floristic region: Evolution and conservation of a global hot spot of biodiversity. *Annu Rev Ecol Evol Syst* 35:623–650.
34. Cowling RM, Witkowski ETF, Milewski AV, Newbey KR (1994) Taxonomic, edaphic and biological aspects of narrow plant endemism on matched sites in Mediterranean South Africa and Australia. *J Biogeogr* 21(6):651–664.
35. Beard JS, Chapman AR, Gioia P (2000) Species richness and endemism in the Western Australian flora. *J Biogeogr* 27(6):1257–1268.
36. Cowling RM, Lombard AT (2002) Heterogeneity, speciation/extinction history and climate: Explaining regional plant diversity patterns in the Cape Floristic Region. *Divers Distrib* 8(3):163–179.
37. Fox MD (1994) Australian Mediterranean vegetation: Intra- and intercontinental comparisons. *Ecology and Biogeography of Mediterranean Ecosystems of Chile*, eds Arroyo MTK, Fox MD, Zedler PH (Springer, New York), pp 137–159.
38. Keeley JE, Fotheringham CJ (2003) Species-area relationships in Mediterranean-climate plant communities. *J Biogeogr* 30(11):1629–1657.
39. Sniderman JMK, Haberle SG (2012) Fire and vegetation change during the Early Pleistocene in southeastern Australia. *J Quat Sci* 27(3):307–317.
40. Tomasovych A, Kidwell SM (2009) Fidelity of variation in species composition and diversity partitioning by death assemblages: Time-averaging transfers diversity from beta to alpha levels. *Paleobiology* 35(1):94–118.
41. Jost L (2007) Partitioning diversity into independent alpha and beta components. *Ecology* 88(10):2427–2439.
42. Veech JA, Summerville KS, Crist TO, Gering JC (2002) The additive partitioning of species diversity: Recent revival of an old idea. *Oikos* 99(1):3–9.
43. Veech JA, Crist TO (2010) Diversity partitioning without statistical independence of alpha and beta. *Ecology* 91(7):1964–1969.
44. Adler PB, et al. (2005) Evidence for a general species-time-area relationship. *Ecology* 86:2032–2039.
45. Layou KM (2007) A quantitative null model of additive diversity partitioning: Examining the response of beta diversity to extinction. *Paleobiology* 33:116–124.
46. Holland SM (2010) Additive diversity partitioning in palaeobiology: Revisiting Sepkoski's question. *Palaeontology* 53:1237–1254.
47. Chao A, Shen T-J (2003) Nonparametric estimation of Shannon's index of diversity when there are unseen species in a sample. *Environ Ecol Stat* 10:429–443.
48. Beck J, Schwanghart W (2010) Comparing measures of species diversity from incomplete inventories: An update. *Methods Ecol Evol* 1:38–44.
49. Manly BFJ (1991) *Randomization and Monte Carlo Methods in Biology* (Chapman & Hall, London).

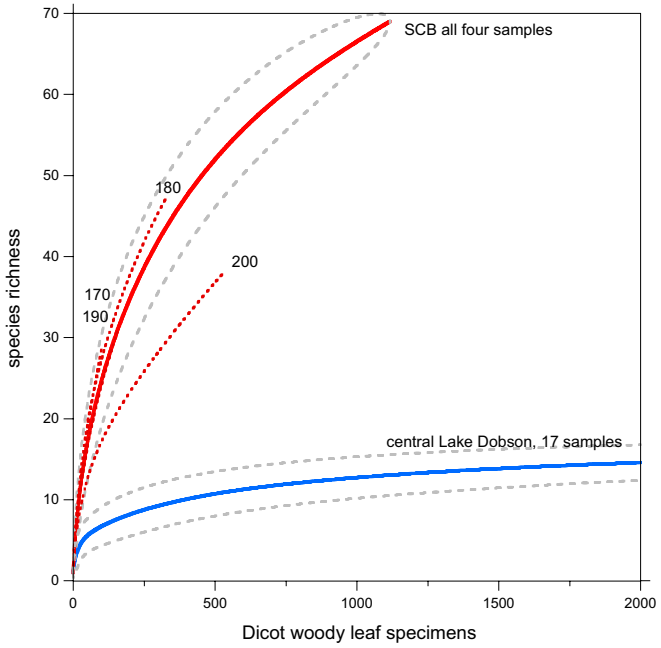

Fig. S1. Rarefaction sampling curves for SCB (individual samples and pooled flora) and central LD (pooled flora of 17 samples).

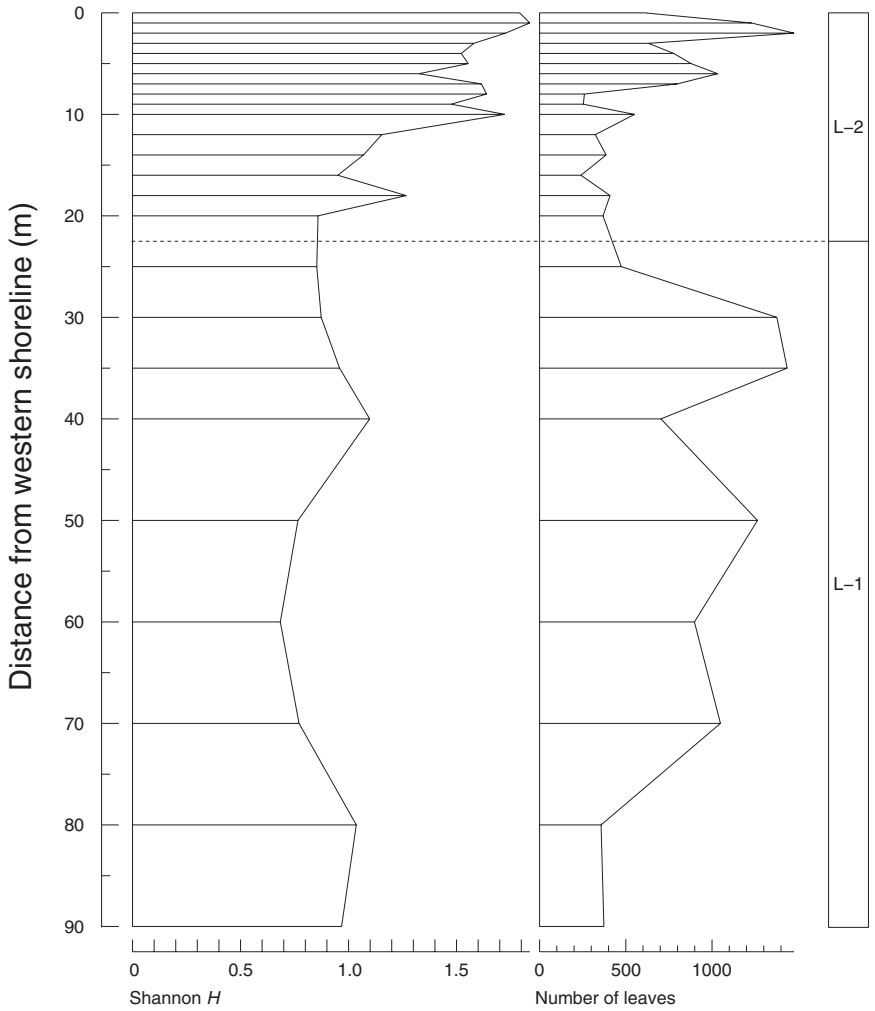

Fig. S2. Shannon diversity *H* and sample size of samples along transects at LD. Spatially constrained zonation executed using optimal splitting by information content in psimpoll 4.27 (available at http://www.chrono.qub.ac.uk/psimpoll/psimpoll.html).

Table S1. SCB fossil flora diversity statistics

	SCB				
Statistic	170	180	190	200	All samples (n = 4)
S	31	47	29	38	69
f_1	17	21	18	21	23
f_2	4	7	5	3	6
f_3–f_{10}	6	12	4	5	25
n	159	325	103	531	1,118
CVr	0.886	1.010	1.082	1.170	0.646
Estimator	ACE-1	ACE-1	ACE-1	ACE-1	ACE
$\hat{S}$	86.2	111.4	124.7	182.2	90.5
$\hat{S}$, SE	38.1	36.4	66.4	99.3	9.8
$\hat{S}$, 95% CI	47–219	70–228	57–356	81–527	78–119
M–M	—	—	—	—	106.8
m	—	—	—	—	13,749
$m_{0.95}$	—	—	—	—	4,401

CVr, coefficient of variability of rare species (1); estimator, ACE (where CVr < 0.8) or ACE-1 (where CVr ≥ 0.8) (1); f_x, number of species represented by x specimens; m, estimated number of additional specimens required to reach asymptotic richness (2); $m_{0.95}$, estimated number of additional specimens required to reach 95% of m; M–M, Michaelis–Menten functional extrapolation of rarefaction (3) calculated using the package EstimateS 8.2.0 (4); n, number of woody dicot leaf specimens; S, observed woody dicot fossil species richness; $\hat{S}$, value of asymptotic estimate of S; $\hat{S}$, SE, SE of $\hat{S}$; $\hat{S}$, 95% CI, 95% CI of $\hat{S}$.

1. Chao A, Shen T-J (2010) *Program SPADE (Species Prediction and Diversity Estimation) Program and User's Guide*. Available at http://chao.stat.nthu.edu.tw. Accessed July 10, 2011.
2. Chao A, Colwell RK, Lin C-W, Gotelli NJ (2009) Sufficient sampling for asymptotic minimum species richness estimators. *Ecology* 90(4):1125–1133.
3. Raaijmakers JGW (1987) Statistical analysis of the Michaelis-Menten equation. *Biometrics* 43(4):793–803.
4. Colwell RK (2005) *EstimateS: Statistical estimation of species richness and shared species from samples. Version 8.2.0. User's Guide and application available at http://purl.oclc.org/estimates.*

Table S2. Leaf assemblage diversity statistics for LD and Lady Lake (1)

	LD S_{veg} = 58 species			Lady Lake S_{veg} = 52 species		
Statistic	Central samples (n = 17)	Margin samples (n = 57)	All samples (n = 74)	Transect 1 (n = 6)	Transect 2 (n = 10)	Transect 3 (n = 6)
S	17	20	20	21	16	10
f_1	2	1	1	6	5	4
f_2	1	1	1	2	3	1
f_3–f_{10}	5	2	1	13	8	5
n	6,153	12,005	18,158	—	—	—
CVr	0.577	0.622	0.860	0.529	0.824	0.665
Estimator	ACE	ACE	ACE-1	ICE	ICE_{th}	ICE
$\hat{S}$	18.2	20.7	21.6	24.6	20.7	13.5
$\hat{S}$, SE	1.8	1.4	3.5	1.6	4.2	1.5
$\hat{S}$, 95% CI	17–27	20–28	20–42	23–29	17–37	12–18
$\hat{S}/S_{veg}$	0.314	0.357	0.372	0.473	0.398	0.260
M–M	17.5	19.6	19.6	—	—	—
m	16,568	NA	NA	—	—	—
$m_{0.95}$	4,581	NA	NA	—	—	—
Rarefied S	13.0	17.0	16.7	—	—	—

LD data rarefied to the sample size of the SCB fossil flora (n = 1,118). CVr, coefficient of variability of rare species (for ACE) or infrequent species [for ICE (incidence-based coverage estimator) and ICE_{th}] (2); estimator, ACE or ICE, where CVr < 0.8, or ACE-1 or ICE_{th}, where CVr ≥ 0.8 (2); f_x, number of species represented by x specimens; m, estimated number of additional specimens required to reach asymptotic richness (3); $m_{0.95}$, estimated number of additional specimens required to reach 95% of m; M–M, Michaelis–Menten functional extrapolation of rarefaction (4) calculated using the package EstimateS 8.2.0 (5); n, number of woody dicot leaf specimens; NA, calculation fails when f_1 = 1; S, woody dicot species richness; S_{veg}, woody dicot species richness of source vegetation; $\hat{S}$, value of asymptotic estimate of S; $\hat{S}$, SE, SE of $\hat{S}$; $\hat{S}$, 95% CI, 95% CI of $\hat{S}$.

1. Drake H, Burrows C (1980) The influx of potential macrofossils into Lady Lake, north Westland, New Zealand. *N Z J Bot* 18(2):257–274.
2. Chao A, Shen T-J (2010) *Program SPADE (Species Prediction and Diversity Estimation) Program and User's Guide*. Available at http://chao.stat.nthu.edu.tw. Accessed July 10 2011.
3. Chao A, Colwell RK, Lin C-W, Gotelli NJ (2009) Sufficient sampling for asymptotic minimum species richness estimators. *Ecology* 90(4):1125–1133.
4. Raaijmakers JGW (1987) Statistical analysis of the Michaelis-Menten equation. *Biometrics* 43(4):793–803.
5. Colwell RK (2005) *EstimateS: Statistical estimation of species richness and shared species from samples. Version 8.2.0. User's Guide and application available at http://purl.oclc.org/estimates.*

Table S3. Analysis of covariance of regional woody dicot species/area datasets and estimates of the woody dicot species richness of SCB source vegetation

Estimate of SCB source richness	F	*P*
SCB/central LD (288 species)		
Southeast Australia	72.41	**<0.001**
SWFR	10.18	**0.002**
CFR	5.68	**0.022**
SCB/central LD, 95% CL_L (179 species)		
Southeast Australia	29.67	**<0.001**
SWFR	1.53	0.220
CFR	0.48	0.493

Within each region, area is a continuous independent variable, woody richness is a dependent variable, and estimated SCB source richness is a categorical independent variable. Results are shown for the best estimate of Early Pleistocene SCB source richness (288 species) and its lower 95% confidence limit (CL_L). Significant differences between species/area curves and estimates of Early Pleistocene SCB source richness at the 0.05 level are shown in bold.

Table S4. Relationship between intersample stratigraphic distance (in centimeters) and the measures of intersample similarity, classic Shannon β-diversity H_β, numbers equivalent of Shannon diversity $D(H_\beta)$, Jaccard similarity, and adjusted Jaccard similarity (1)

Measure	Ordinary least squares regression	R^2	*P*
H_β	$0.2355 - 0.0059x$	0.120	0.501
$D(H_\beta)$	$1.2735 - 0.007x$	0.130	0.483
Jaccard similarity (classic)	$0.6465 + 0.00128x$	0.005	0.896
Jaccard similarity (adjusted)	$0.8315 + 2.7478\ E\text{-}18x$	0.000	—

Jaccard similarities calculated in EstimateS 8.2.0 (2). None of the relationships are significant at the $P = 0.05$ level.

1. Chao A, Chazdon RL, Colwell RK, Shen TJ (2005) A new statistical approach for assessing similarity of species composition with incidence and abundance data. *Ecol Lett* 8(2):148–159.
2. Colwell RK (2005) *EstimateS: Statistical estimation of species richness and shared species from samples. Version 8.2.0. User's Guide and application available at http://purl.oclc.org/estimates.*

Table S5. Shannon diversities of SCB samples

	H	$\hat{H}$
H_α sample 170	2.494	2.726
H_α sample 180	2.844	3.001
H_α sample 190	2.408	2.775
H_α sample 200	2.089	2.207
Mean H_α	2.459	2.684
H_γ	2.634	2.709
$H_\beta = H_\gamma - H_\alpha$	0.175	0.025
$D(H_\beta) = \exp(H_\beta)$	1.192	1.026
H_β *p* (bootstrap)	0.097	0.312

P values calculated as the percentile of the distribution from a 1,000-sample bootstrap simulation. *H*, classical or maximum likelihood estimator of Shannon diversity; $\hat{H}$, estimator of *H* (1).

1. Chao A, Shen T-J (2003) Nonparametric estimation of Shannon's index of diversity when there are unseen species in a sample. *Environ Ecol Stat* 10(4):429–443.

Other Supporting Information Files

SI Appendix (PDF)